DETERMINATION OF PROJECTILE PROTON BEAM ENERGY FOR THE BEST YIELD OF As-ISOTOPES FROM Ge-CRYSTAL

by

Genene Tessema

A Thesis

Submitted in Partial Fulfillment for the Requirements

for the Degree of Master of Science in Physics

in the Addis Ababa University

June, 1995

School of Graduate Studies

Addis Ababa University

Addis Ababa

ACKNOWLEDGEMENT

I am extremely grateful to Dr. R. Vianden who allowed me to join his research group in the Institut für Strahlen-und Kernphysik, University of Bonn, Germany. I am really indebted to his constant advise throughout my work in the institute.

I would like to express my gratitude to Giudo M., Peter F., Maria W., Giudo W., Uwe and Christoph D. for their unreserved assistance and hospitality they provided me during my stay in Germany.

It is my pleasure to express my due thanks to Prof. J. Bisplinghoff, Institut für Strahlen-und Kernphysik, University of Bonn, who helped me to find an advisor in the research area which I am interested to work in.

My gratitude extends to my home advisor Dr. S. Tesch, Addis Ababa University, for his constructive criticism and comments he gave me in the preparation of the thesis.

On behalf of the Alemaya University of Agriculture, I want to extend my appreciation to the Deutscher Akademischer Austauschdienst (German Academic Exchange Service, DAAD) for the financial support I received during my stay in Germany, without which the work would not have been possible.

Finally, I would like to express my thanks to Ms. Elizabeth Yohannes, who typed the first draft of the thesis. I am also thankful to Negussie Terfessa for his constant encouragement to complete the work within a relatively short period.

ABSTRACT

To extract information for the appropriate proton beam energy, which will be used for irradiating natural Ge crystal for the best yield of As isotopes, is the mere objective of this work. Five slices of natural Ge crystal with various thickness have been prepared in order to make energy degradation, and a proton beam energy of 35MeV is set to be incident onto the first slice. After irradiation measurements have been taken from each slice using a Ge(Li) detector, and spectral analysis are also carried out. From the complete spectral analysis and using a computer simulation programme called Transport of Ions in Matter (TRIM) the projectile proton beam energies are determined for the best yield of ^{71}As, ^{72}As, ^{74}As, ^{76}As, ^{69}Ge, and ^{67}Ga isotopes.

In this thesis the experimental results are discussed, and calculations are carried out for the cross-sections of the observed reaction product. From the dependence of the cross-section versus projectile beam energy, extrapolation is made to estimate the corresponding threshold energy for the reactions to occur.

CONTENT

5. Data Analysis and Discussion

INTRODUCTION

Beginning from the last three decades, the development of semiconductor technology highly depends on ion-implantation technique, which enables one to put or create desired amount of elements into a given solid. That is, the technique can be applied to changing a wide range of physical and chemical properties of the target solid. One way of implanting ions into solids is to use an accelerator to produce charged particle beam with sufficiently high kinetic energy. Such a beam of charged particles can cause nuclear reactions when it bombards a solid target. The technique is broadly classified into two categories depending on the type of ions used that is, light and heavy ion implantation. Ion implantation offers a number of technological advantages which are important in the fabrication of electronic devices, and in studies of surfaces in solid state physics. Of course, during irradiation energetic particles cause crystal defects, which are generally undesirable because of changes in the electrical and optical properties of the solid. However, this problem can largely be solved by annealing the sample after irradiation.

The work in this thesis is aimed at obtaining information on high value of the reaction cross-section for the production of As isotopes from natural Ge crystals target, irradiated by proton beam in a chosen energy range of interest. Particularly, interest has been put to the yield of ^{71}As which results in the production Ga-antisite defect in the target. Energy degradation has been made by preparing different thickness slices of Ge crystals, which were put together in a target holder. After irradiation measurements were taken from each Ge samples under the same experimental conditions, and independent analysis is also carried out.

The reason for why it is required to produce ^{71}As isotopes in Ge crystal was, to generate defects like single acceptors [$^{71}Ge_{As}$] and Ga-antisite defects [$^{71}Ga_{As}$] which are

double acceptors created as a consequence of the following decay scheme (^{71}As---65h------>^{71}Ge ----11.2d----->^{71}Ga). The high yields of these defects will enable those researchers, who are engaged in the investigation of the property of semiconductors, to study the microscopic behaviour of these defects in germanium crystal.

This thesis contains a description of the interaction of electromagnetic radiation with matter and a brief discussion about nuclear reactions. Besides, it includes the working principle of lithium drifted germanium [Ge(Li)] detectors and a short summary of the cyclotron used. Finally, the results of the experiment and the corresponding conclusions are presented.

where I_0 : incident beam intensity

x : thickness of absorber

μ : absorption coefficient

The absorption coefficient is a quantity which is characteristic of the absorbing material and γ-energy is directly related to the total absorption cross-section.

The probability of any incident photon initiating any of these processes can be expressed as a cross-section per atom ; the probability for a photon interacting at all would be the total cross-section, being the sum of the individual cross-sections. If we multiply the total cross-section per atom by the number of atoms per unit volume, we obtain the linear attenuation coefficient μ, which is a measure of the number of photons removed by one of these processes from a beam of photons per unit path length in the absorbing medium.

1.1 PHOTO-ELECTRIC EFFECT

The photo-electric effect (fig.1.1) involves complete absorption of a photon by an atomic electron with the subsequent ejection of the electron from the atom. If the energy of the photon is sufficiently high the electron is ejected from the atom with a kinetic energy given by

$$K = h\nu - I \qquad (1.1)$$

where $h\nu$ is the energy of the incident photon, and I is the binding energy of the electron in the atom.

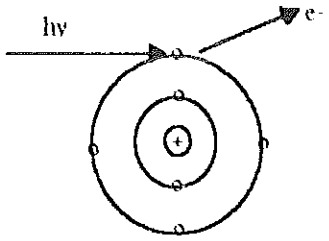

Fig.1.1 Schematic diagram describing the photo-electric effect.

The process as whole is known as the photo-electric effect, and the ejected electron is called photo-electron. The γ-rays, which we are mainly interested in, have high energies compared with the binding energy of those of orbital electrons. Therefore, for high-energy radiation even the electrons near to the nucleus have a large probability of ejection. Moreover, ionisation energy is largest for electrons near the nucleus and increases with atomic number.

Most of the photo-electrons are emitted in the direction nearly perpendicular to that of the incident radiation. Particularly, for polarised radiation the photo-electrons are mainly emitted in the direction of the electric field vector. There is, however, a certain preference for a forward rather than a backward direction for the photo-electrons. That is, the maximum emission is at an angle less than 90^0 to the direction of the incident radiation. This phenomenon can be explained qualitatively by the fact that most of the momentum $h\nu/c$ of the incident light quanta is transferred to the photo-electrons and, the remaining of the momentum is carried away by the recoiling atom. However, because of large mass of the recoiling atom as compared to the mass of the electron, it receives practically none of the energy. As an illustration the angular distribution of photo-electrons ejected is shown in fig1.2 for two energies of the primary radiation.

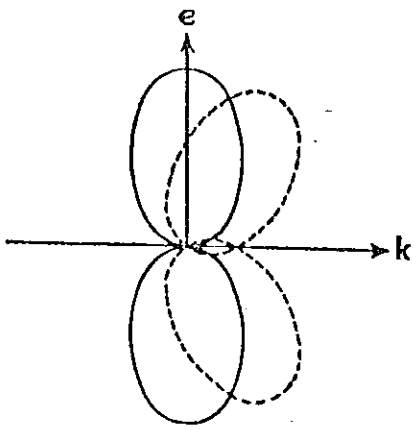

Fig.1.2 Angular distribution of photo-electrons. The figure shows the distribution of photo-electrons with low velocity (solid line) and with velocity $V = \frac{1}{3}c$ (broken line). The arrows k and e mark the directions of the primary radiation and of the electric field vector (ref.10).

From quantum mechanical calculations, it is found that the probability of photo-electric absorption (per atom of the absorber), varies approximately in proportion to the atomic number and the incident energy, according to

$$\sigma_{ph} \propto \frac{Z^5}{(h\nu)^{7/2}} \qquad (1.2)$$

Thus, the probability of photoabsorption increases very rapidly with atomic number and decreases rapidly with energy. In other words, the photo-electric effect is stronger for lower energy γ-rays and for absorber materials of high atomic number. For this reason materials with large Z are better for shielding purposes and for detection of gamma-rays, especially, where energy measurements are to be made.

1.2 COMPTON SCATTERING

Unlike the photo-electric effect, which can only occur with strongly bound electrons, Compton scattering is an interaction between photons of electromagnetic radiation and free or only weakly bound electrons. During interaction the photon transfers only part of its energy to the electron and is scattered with lower energy.

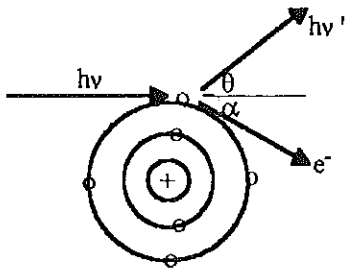

Fig1.3 Illustrative diagram for Compton scattering .

From the law of conservation of energy and momentum one can arrive at the following relation for the energy of the scattered photon as a function of the scattering angle θ, namely

$$E_\gamma' = \frac{E_\gamma}{1 + \frac{E_\gamma}{m_o c^2}(1 - \cos\theta)} \qquad (1.3)$$

The remaining energy of the incident photon goes to the electron kinetic energy. The maximum recoil energy allowed by kinematics for the electron is when scattering occurs at angle $\theta = 180^0$. Substituting this value for θ one obtains the following expression for kinetic energy (T) of the electron

For $\theta = 180^0$ $\qquad T = h\nu\left(\frac{2\zeta}{1+2\zeta}\right)$ $\qquad (1.4)$

where $\zeta = \frac{h\nu}{m_0 c^2}$

This maximum recoil energy is known as the Compton edge energy. The cross section for Compton scattering was one of the first to be calculated using quantum electrodynamics, and

is known as Klein-Nishina formula. According to this relation the total probability per electron for Compton scattering to occur is

$$\sigma_c = 2\pi r_e^2 \left[\frac{1+\zeta}{\zeta^2} \left\{ \frac{2(1+\zeta)}{1+2\zeta} - \frac{1}{\zeta}\ln(1+2\zeta) \right\} + \frac{1}{2\zeta}\ln(1+2\zeta) - \frac{1+3\zeta}{(1+2\zeta)^2} \right] \qquad (1.5)$$

where $\xi = \frac{h\nu}{m_e c^2}$ and r_e is the classical electron radius

From the theoretical cross-section for electrons, the number of scattering collisions per cm of path in a material can be deduced at once by multiplying the cross-section by the number of electrons per cm^3 of the material (NZ).

However, most of the Compton-scattered photons go in the forward direction, that is in the direction of the incident photon, especially, for incident energies above 100 keV. This is illustrated in fig.1.4 for the angular distribution of intensity of the scattered photons.

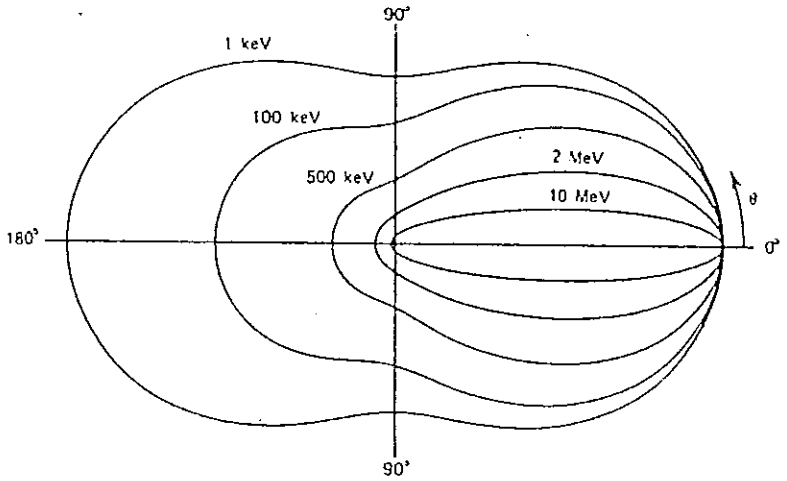

Fig1.4 A polar plot of the number of photons (incident from the left)

Compton scattered into a unit solid angle at the scattering angle θ.

The curves are shown for the indicated initial energies.

1.3 PAIR PRODUCTION

The process of pair production involves the transformation of a photon into an electron-positron pair. The law of conservation of momentum and energy requires pair production to occur only in the presence of a third body, that is in the field of a charged particle, such as an atomic nucleus. Besides, the conservation of energy requires a minimum photon energy of 1.022 MeV (i.e. twice of the rest mass energy of the electron) for the process to occur. If the original photon has an energy greater than this threshold value, it is still used up completely in the pair production process. The residual energy now appears as the kinetic energy of the newly created particles. In general the residual energy is not equally shared between them.

Furthermore, no simple expression exists for the probability of pair production per nucleus, but its magnitude varies approximately as the square of the absorber atomic number. Besides, the role of the pair production process rises sharply with increasing energy. Using the Born approximation together with analytical integration, the following expression is found for the total cross-section of pair production in which screening effects are not considered.

$$\sigma_{pp} = \frac{Z^2 r_e^2}{137}\left\{\frac{28}{9}\ln\frac{2E_\gamma}{m_e c^2} - \frac{218}{27}\right\} \qquad (1.6)$$

for $m_e c^2 << E_\gamma << 137 m_e c^2 Z^{-1/3}$ (ref.23).

1.4 TOTAL ABSORPTION COEFFICIENT AND PHOTON ATTENUATION

Consider the following simple experiment as an illustration for attenuation of radiation. Suppose monoenergetic γ-rays are collimated into a narrow beam and allowed to strike a detector after passing through an absorber of variable thickness, the result should be

simple exponential attenuation of the gamma rays as shown in fig.1.5. Each of the interaction processes discussed in the last sections removes a gamma ray photon, from the beam either by absorption or scattering away from the detector direction and can be characterised by a fixed probability of occurrence per unit path length in the absorber. The sum of these probabilities is simply the probability per unit path length that the gamma-ray photons are removed from the beam.

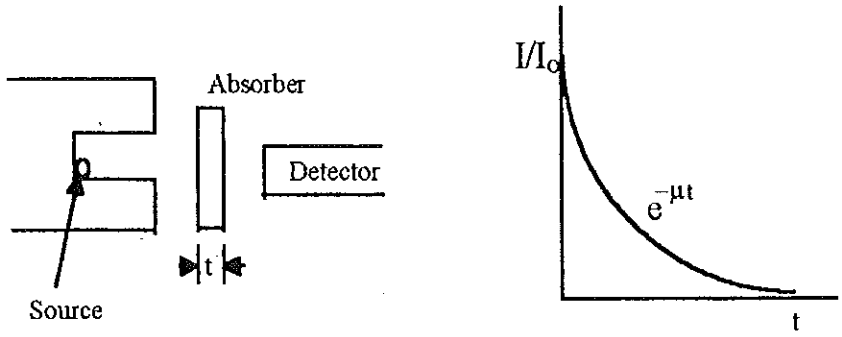

Fig1.5 Schematic diagram for photon attenuation measurement

The total probability for photon interaction in matter is the sum of the individual cross-sections outlined above. If one calculates the cross-section per atom, it takes the form

$$\sigma = \sigma_p + Z\sigma_c + \sigma_{pp} \tag{1.7}$$

where we have multiplied the Compton cross section by Z to take into account the Z electrons per atom. If we now multiply σ by the density of atoms (N), we obtain the probability per unit length for an interaction.

$$\mu = N\sigma = \sigma(\frac{N_a \rho}{A}) \tag{1.8}$$

where N_a : Avogardo number

ρ : density of the absorber

A : molecular weight.

The quantity μ is more commonly known as the total absorption coefficient and is just the inverse of the mean free path of the photon. The mean free path is defined as the average distance travelled in the absorber before an interaction takes place. Its value can be obtained from relation

$$\lambda = \frac{\int_0^\infty x\, e^{-\mu x} dx}{\int_0^\infty e^{-\mu x} dx} = \frac{1}{\mu} \qquad (1.9)$$

From this it follows that the fraction of photons surviving a distance x is then

$\frac{I}{I_0} = e^{-\mu x}$ where I_o is the incident intensity.

Fig1.6 describes the behavior of the total photon absorption cross-section for germanium, and from this figure the following statements can be derived. At low energies the photo-electric effect plays the dominant role, and then, roughly speaking between energies 0.3 MeV - 6.0 MeV the Compton scattering is dominant and above 6.0 MeV pair production plays an important role in the interaction process.

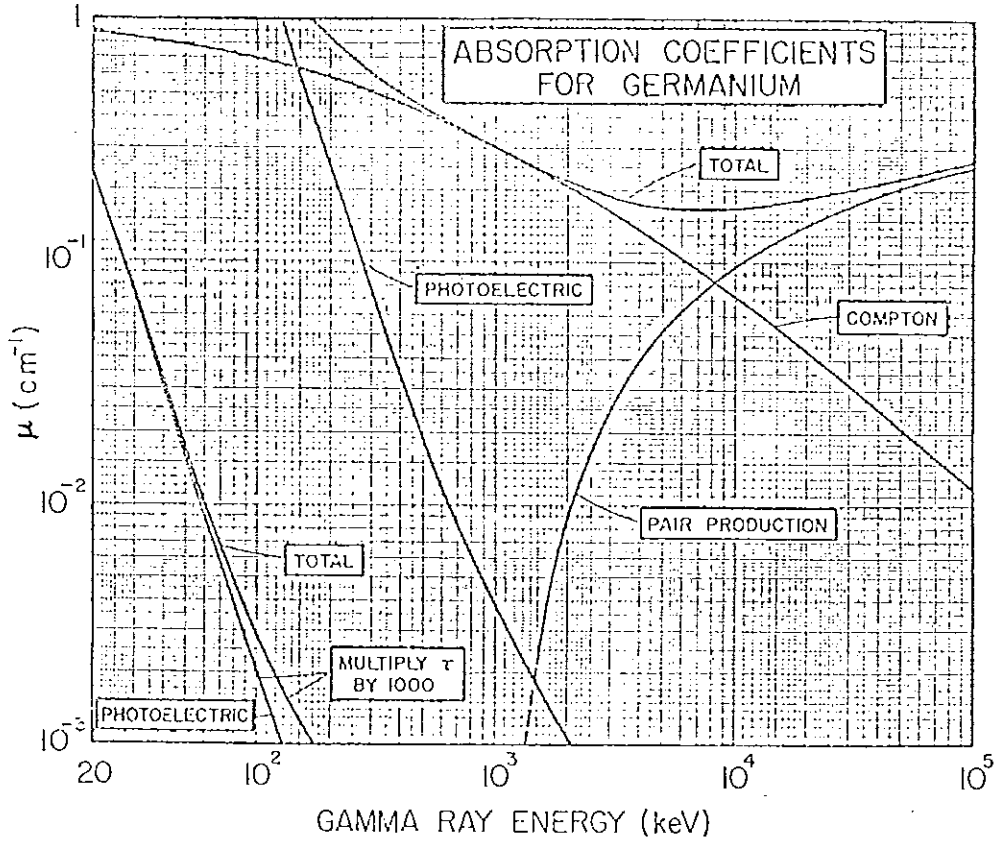

Fig.1.6 Absorption coefficient for germanium

CHAPTER II

LITHIUM-DRIFTED GERMANIUM DETECTOR Ge (Li)

Introduction.

The primary advantage of semiconductor detectors over other detectors are the very small average energy needed to create an electron-hole pair. Like gases, the average energy to create an electron-hole pair at a given temperature is found to be independent of the type and energy of the radiation, and only dependent on the type of the material. For gaseous detectors the average energy to create an ion-electron pair is nearly 30eV(ref.7). But, the average energy for electron-hole creation in silicon and germanium is much less than this value. These values are listed in the following table.

Table 2.1 Values for average energy of electron- hole pair creation in Si and Ge (ref.2).

Temperature	Si	Ge
300^0 K	3.62eV	----
77^0 K	3.76eV	2.96eV

For the same radiation energy, the number of charge carriers created is therefore almost an order of magnitude greater in semiconductors than in gases. Compared to the number of photo-electrons created in a scintillation counter, this increase approaches two orders of magnitude. On the other hand, for gamma-ray detection, germanium is preferred over silicon because of its much higher atomic number (Z_{Si} = 14 ; Z_{Ge} = 32). The photoelectric cross-section is thus about 60 times greater in Ge than in Si. However, germanium must be operated at low temperatures because of its smaller band gap (≈0.7 eV), otherwise electrons from the valence band jump easily to the conduction band by thermal agitation, so that the resulting effect disturbs the detection of the signal caused by the radiation.

In order to obtain a sufficiently sensitive thickness for the detection of gamma rays, the first detectors were made from lithium compensated. These detectors are known as lithium drifted germanium [Ge(Li)] detectors. Maximum obtainable thickness for compensated germanium are about 15 to 20mm, therefore, a coaxial geometry is generally used to maximise the sensitive volume.

2.1 BASIC PRINCIPLE FOR CONSTRUCTING SENSITIVE REGION OF Ge(Li) DETECTOR AND LITHIUM CONCENTRATION.

Most Ge(Li) detectors which are in use today are fabricated from a cylindrical p-type crystal of germanium of large volume, typically 50 cm^3 or greater. In order to create compensated region in the p-type germanium crystal, lithium is coated onto the cylindrical surface and drifted towards the centre under the action of heat and electric field to create an effectively intrinsic region surrounding a cylindrical p-type core. In germanium a lower drift temperature ($\sim 50^0$C) is used than in silicon and must be followed by a "clean up" at a temperature (-10^0C to 0^0C) to improve compensation.

Since lithium is an alkali metal and has one valance electron, it can easily give up the valence electron to neutralise an acceptor site, and prevents holes being created in the valence band. The effect is to turn the layer over which the lithium has been drifted into an electrically intrinsic region by neutralisation of the acceptor atoms.

Fig.2.1 and fig.2.2 shows the basic structure of the sensitive region of a Ge(Li) detector, and the general behaviour of lithium concentration in the whole region of the crystal.

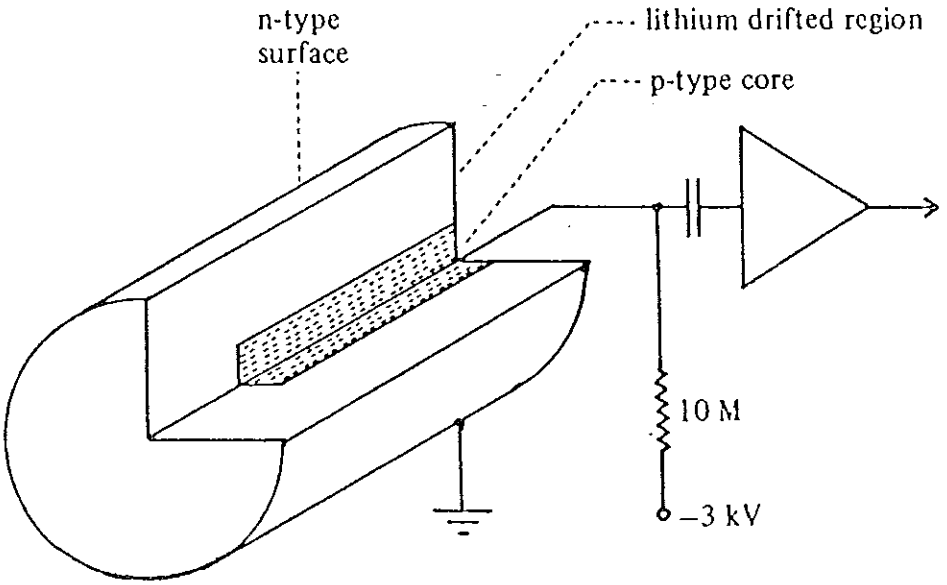

Fig.2.1 Lithium drifted germanium (Ge(Li)) detector.

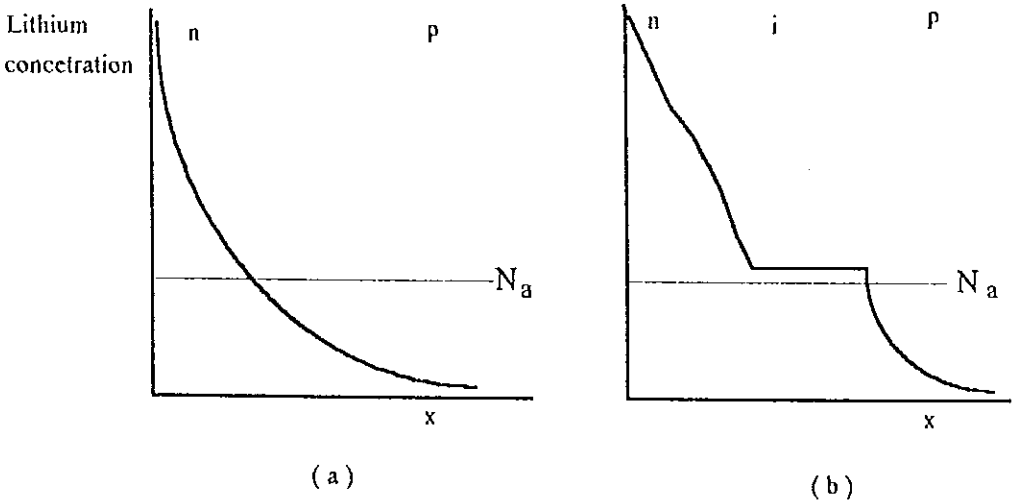

Fig2.2 The lithium drift process: a) after diffusion b) after drifting.

(N_a is the acceptor concentration.)

As shown in the fig.2.2 the lithium is not drifted all the way through the crystal, so that a p-type region remains. Electrode connection is made to this via an evaporated aluminium contact. On the other hand, at the front surface there will be excess lithium atoms. thus producing a thin region in which the majority carrier will be electrons and this can be regarded as a thin n-type region. Again the opposite sign of the electrode is connected to this n-region with a thin evaporated gold layer.

After completion of the lithium drift, the detector must be kept at a low temperature, otherwise because of the high mobility of the lithium ions in germanium, even at room temperature and without an electric field they tend to diffuse to fill lattice vacancies, resulting in a significant loss in sensitivity and resolution, which can be repaired only partially by clean-up drift .

2.2 COOLING SYSTEM OF THE DETECTOR

It is customary to mount lithium-drifted germanium detector on a "cold finger" that is a metal base which is constantly cooled by liquid nitrogen. One such arrangement is shown in fig.2.3, which consists of dewar, vacuum chamber, metallic rod one end of which is immersed in liquid nitrogen and the other end carries the detector with its preamplifier. The detector can be mounted above or below a dewar flask, as an illustration of the cooling system of the detector in fig.2.3 use is made from the type in which the detector is mounted above the dewar flask. Of course, the working principles in both cases are identical.

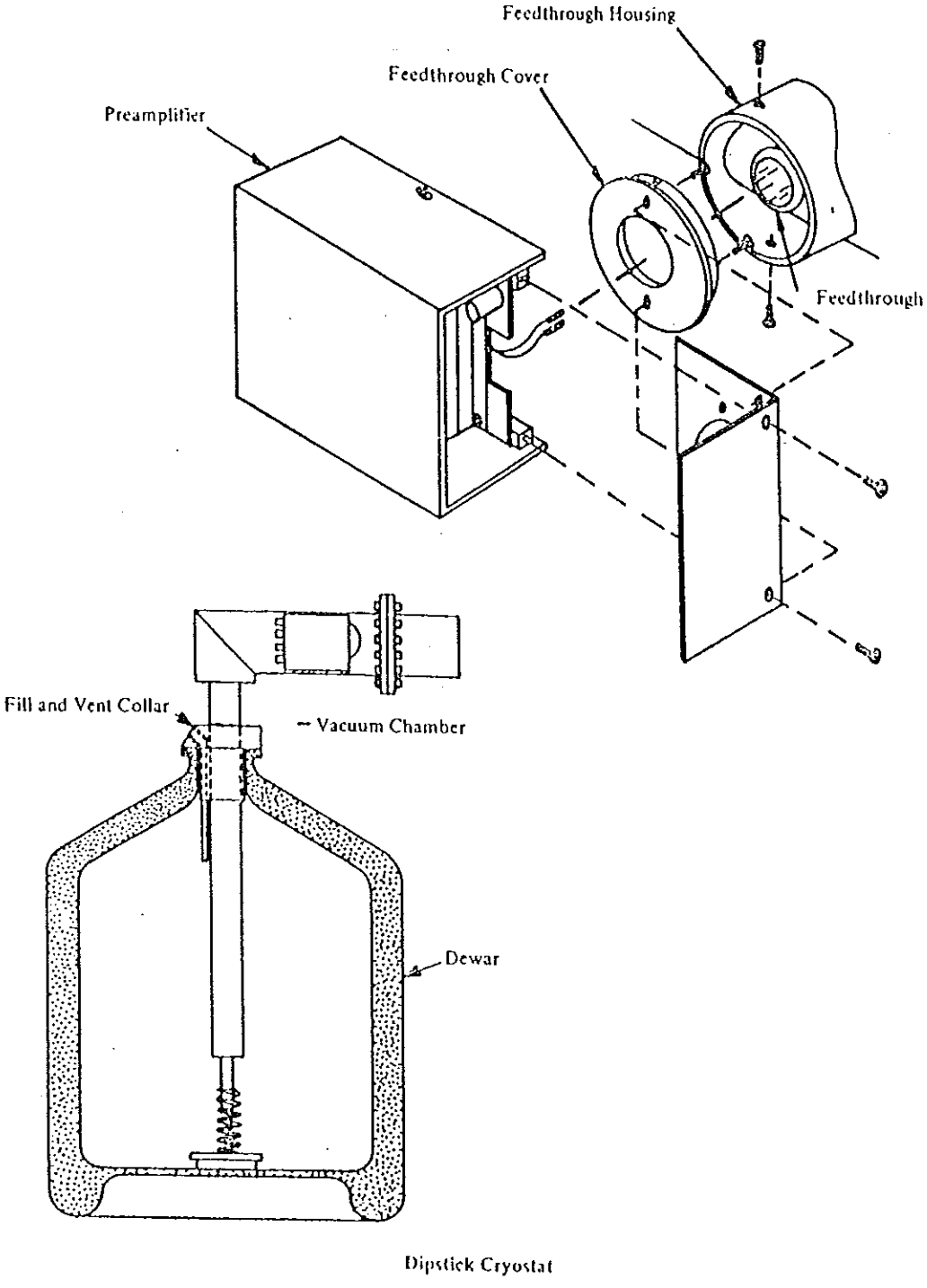

Fig.2.3 Cooling system of the Ge(Li) detector with its preamplifier.

As it is clearly seen from the figure, the preamplifier is placed as closely as possible to the detector, in order to reduce cable resistance for the signal coming out of the detector.

2.3 DETECTOR SPECIFICATIONS

All spectral measurements in this work are carried out with t he detector having the following specifications

1. Geometry

   Cylindrical with outer diameter of 51mm

   Length 39.00mm

   Coaxially drifted p- core with diameter 9mm

   Weight 424g

   Distance from window 7mm

   Sensitive volume 60cm^3

2. Cryostat/ Dewar : HLC , 15 liter
3. Preamplifier type : 2001 Canberra model 970
4. Shaping time : 4μsec
5. Advised voltage, (-) 3500 Volt
6. Resolution and peak to Compton ratio, as given in table 2.2

Table 2.2 Resolution and peak to Compton ratio of the detector

ISOTOPE	^{57}Co	^{137}Cs	^{60}Co	^{228}Th
Energy (keV)	122	662	1332	2614
Half-width(keV)	1.0	1.5	2.0	3.0
Tenth-width (keV)	1.9	2.85	3.8	5.85
Peak/Compton	---	54:1	34:1	27:1

2.4 THE ELECTRONICS SYSTEM USED

In general, signals obtained from semiconductor detectors are very small. Therefore, care must be taken to use low-noise electronics for signal processing. In particular, a preamplification is necessary before any further treatment can be made. Since the capacitance of semiconductors change with temperature, this is performed by a charge -sensitive preamplifier. This type of preamplifier is preferred because of its insensitivity to changes in capacitance at its input. Besides, to ensure stability, it is necessary for the preamplifier capacitance to be much larger than all other sources of the capacitance at the input, i.e. the detector cables etc. Fig.2.4 shows the spectrometry system used in our measurement.

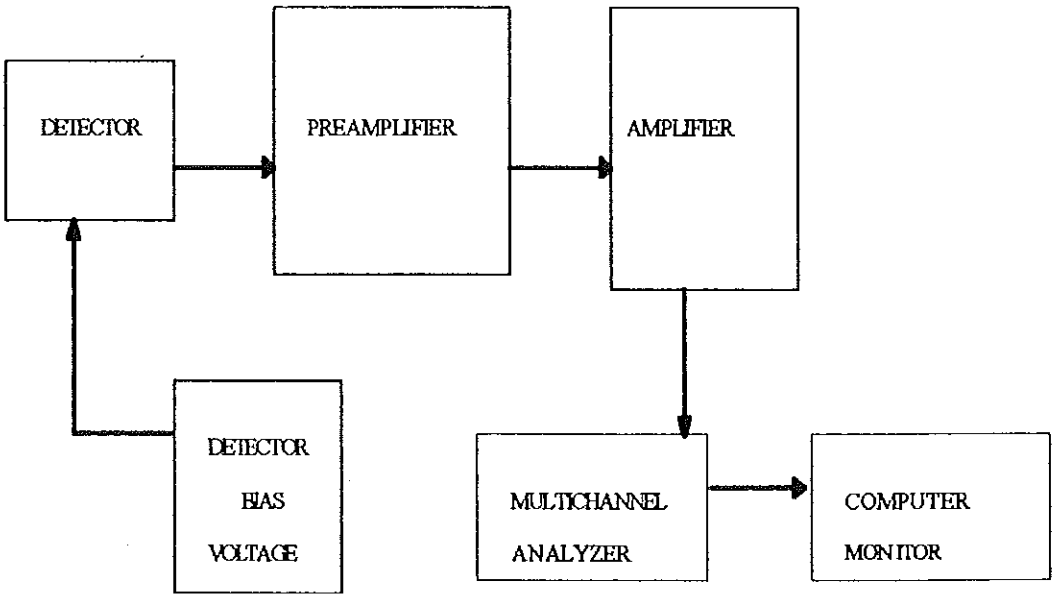

Fig.2.4 Diagram of electronics for the detector.

The preamplifier receives signals from the detector caused by the incident radiation. These signals pass to the amplifier for further amplification up to the order of volts and to shape the pulses so that they will be compatible with the input requirements of the processing modules. Signals from amplifier is sent to multichannel analyser to extract the necessary information about the pulses. For example, a knowledge of the pulse height distribution can give information about the energies and intensities of the incident radiation. Finally, the spectrum is displayed on the computer monitor through ACCUSPEC data acquisition programme.

CHAPTER III

NUCLEAR REACTIONS AND REACTION CROSS-SECTIONS

3.1 NUCLEAR REACTION

In a broad class of nuclear experiments studies are made of collisions of neutrons (n), protons (p), deuterons (d), and a particles with various other nuclides. When the bombarding nucleons is transformed in any way in the collision, the process is called a nuclear reaction : otherwise one speaks of elastic scattering. If the species **A** is bombarded by a particle **a**, to form a nucleus **B** and fragment **b**, the reaction is described by

$$\mathbf{a} + \mathbf{A} \rightarrow \mathbf{B} + \mathbf{b} \qquad (3.1)$$

or more compactly by **A(a,b) B**.

Nuclear reactions can be classified according to the reaction mechanism that provides the most appropriate description. We shall consider three such mechanisms :(1) processes in which the colliding partners temporarily fuse into a single "Compound nucleus" (2) the direct processes in which the contact between partners is only peripheral, and (3) that of distant processes in which the colliding nuclei hardly come into direct contact. It is not desirable to make a full explanation about nuclear reaction here. But, in this chapter a brief discussion of the compound nucleus reaction is presented.

3.2 THE COMPOUND NUCLEUS

Many different kinds of events may occur when a beam of particles strikes a target. One of the most important types of reaction, particularly when the incident particles are of low energy (less than about 50MeV) is compound nucleus (ref.26). The theory of reactions of this type was first discussed by Niels Bohr in 1936.

In the general reaction **A(a,b)B**, the nuclear system consisting of **A** and **a** (or equivalently of B and **b**), is called the compound system of the reaction. The compound nucleus will have, in general, a ground state in which the particle **a** is bound, low excited states which may decay only by gamma radiation, and excited states the energy of which is greater than the separation energy of **a**. These latter states may decay by gamma radiation, emission of **a**, and possibly by the emission of other particles. They are, of course, not stationary, but their lifetimes may be very long compared with the life time of traversal of the particle **a** across the nucleus. They are called quasi-stationary states or "resonance level". In such states the energy is not entirely sharply defined, the energy uncertainty Γ is related to the lifetime τ of the state by $\Gamma\tau = \hbar/2\pi$.

The life time of the compound nucleus is almost invariably too short to be measured with existing instruments and may be of the order of 10^{-18} sec, but it is long enough for energy imparted by the incident particle to be shared among the constituent of the nucleus, a process which may take only about 10^{-21}sec.

At excitation energies in the order tenths MeV, the compound nuclei must be in a chaotic state. Many nucleons will be excited into energy levels well above their normal ground state levels, and the nucleus may contain a considerable amount of rotational and vibrational energy . There will usually be a very large number of closely spaced energy levels. It is then no longer possible to recognise discrete energy levels, and the nucleus no longer exist in a single, well-defined quantum state. Its energy and its angular momentum, of course, remain constant, but there may be an enormous number of different nuclear configurations of the same energy and angular momentum, and the nucleus will oscillate very rapidly between all these different possible states.

Immediately after the formation of the compound nucleus, the system possesses of one of the quasi-stationary states of the compound system. The compound nucleus reaction may

be described as a two step resonance process. The capturing of incident particle and the disintegration of the intermediate state formed as the result of collision process. The probability of capturing of the incident particle varies in a characteristic manner with a difference between the energy E of the colliding system and the energy E_λ of the resonance level. The total cross-section for the process is proportional to the capture probability. The probability varies with energy roughly as

$$[(E - E_\lambda)^2 + (\Gamma/2)^2]^{-1} \qquad (3.2)$$

Where Γ is the energy width of the resonance level (ref.27).

The disintegration of the intermediate state is also governed by the probability laws. The emission of each of the possible products of the collision has a certain probability characteristic of the product and of the resonance level. Thus if the partial widths for proton, neutron, and gamma ray emission from the particular level are $\Gamma_p, \Gamma_n, \Gamma_\gamma$, thus the probability that the disintegration eventually yields a neutron is Γ_n/Γ, where

$$\Gamma = \Gamma_p + \Gamma_n + \Gamma_\gamma \qquad (3.3)$$

is the total width of the compound state.

The effect of the electrostatic barrier manifests itself in a reduction of the Γ for the process inhibited by the barrier. For instance, the electrostatic barrier decreases Γ_p which inhibits the emission of protons from the nuclei.

The compound nucleus is pictured then as a hot liquid or solid from which various particles eveporate. From heavy nuclei, neutrons evaporate most easily even at high energies of excitation but proton emission is also common from lighter nuclei.

3.3 REACTION CROSS-SECTION

A nucleus of radius R will present a target of projected area πR^2 to an incident particle. For a target of A=100, this area will be approximately $\pi(100^{1/3} * 1.2*10^{-13})^2 cm^2$, or about 0.97 barn. The probability that an incident particle will strike the nucleus is proportional to this target area, which of course is equal to the area of a cross-section of the

nucleus through its centre. The cross-section is related with the rate of the production of the isotope during irradiation as follows.

Suppose that n(t) be the number of radioactive nuclei created at time t during irradiation. Let N_t be the number of target nuclei. The rate of change of the number of radioactive nuclei created during irradiation is given by

$$\frac{dn}{dt} = \phi\sigma N_t - \lambda n \tag{3.4}$$

where ϕ and σ are the incident particle beam flux and the cross-section respectively. Integrating this equation yields the number of radioactive nuclei just after irradiation as

$$\int_0^n \frac{dn}{\frac{\phi\sigma N_t}{\lambda} - n'} = \int_0^T \lambda dt \tag{3.5}$$

$$n(T) = \frac{\phi\sigma N_t}{\lambda}(1 - e^{-\lambda T}) \tag{3.6}$$

where T is the period of irradiation.

Therefore, from the last equation the activity just after irradiation is obvious, which takes the form as

$$A(T) = \phi\sigma N_t (1 - e^{-\lambda T}) \tag{3.7}$$

From the spectral measurement of the radioactive isotopes, one can easily determine the activity just after irradiation. The other parameters are data from the experiment, and hence using the equation 3.7 it is obvious to calculate for reaction cross-section.

Therefore, taking into account the composition of the element in the target and the relative amount of each isotopes in percentage, and putting an appropriate unit for all the parameters in the equation, the activity finally reads as

$$A = 1.6 * 10^{-13} * \phi\sigma mrh * \frac{1}{n}(1 - e^{-\lambda T}) \tag{3.8}$$

where A : is the activity in (mCi)

ϕ : is the projectile particle beam flux in $\{\frac{1}{cm^2 sec}\}$. That is the number of incident particles per cm^2 per unit time.

σ : is the cross-section in barn $\{1b = 10^{-24} cm^2\}$

m : is the irradiated target mass in (mg). This reprcsents only the mass of the target bombarded by the incident beam.

r : is the relative contents of the element in the target
(for example Sio_2 crystal the value of r for Si will be $r = \frac{28}{28+2(16)}$)

h : is relative amount of the isotope in [%], in pure Ge crystal, the isotope ^{72}Ge has h = 27.5%

n : is the mass number of target nuclei

CHAPTER IV

EFFICIENCY OF THE DETECTOR, THE SAMPLES AND IRRADIATION FACILITY

4.1 RELATIVE EFFICIENCY OF THE DETECTOR

The most common and quick way to obtain the efficiency of the detector is, to compare the measured intensities from a given source, with the corresponding intensities of the same source measured by a detector of known efficiency. We used europium (^{152}Eu) and barium (^{133}Ba) sources for measuring intensities, which are used to determine the relative efficiency of the detector through EFFIT programme. The EFFIT programme provides the possibility to compute relative efficiency by comparing the normalised measured intensities with the corresponding intensities of the same source taken from Nuclear Data Sheets, which are considered in our measurement as the true intensities of the source. EFFIT was first presented by D.C.Radford on the workshop on "Large γ-ray Detector Arrays" in 1992, the name of the whole programme package is RADWARE, and the programme was found to be good for quantitative measurements in γ-ray spectroscopy.

Once the relative efficiency of the detector at different peak energies are obtained ,the next step is to make a functional fit to all the measured data points. This efficiency fit curve provides the value of the relative efficiency of the detector in a wide energy range. The fit function used was

$$eff = \exp\left\{\left[(A + BX + CX^2)^{-G} + (D + EY + FY^2)\right]^{-1/G}\right\} \qquad (4.1)$$

Where $X = \log(\frac{E_\gamma}{E_1})$ $\quad E_1 = 100$ keV

$Y = \log(\frac{E_\gamma}{E_2})$ $\quad E_2 = 1$MeV

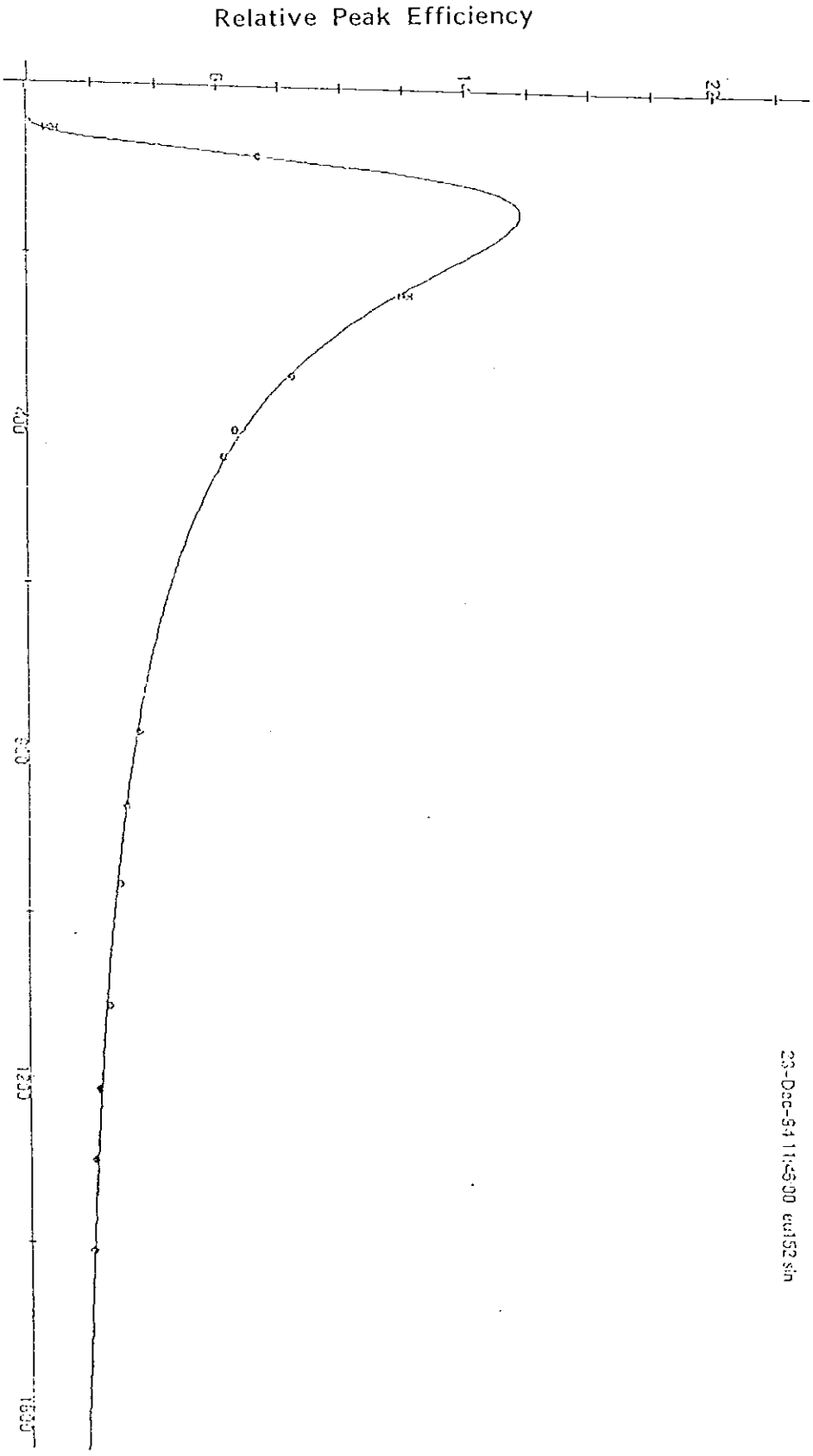

Fig.4.1 Relative peak efficiency of the Detector

The fit parameters found were

A = 5. 1364 ± 0.292
B = 9.2836 ± 1.1002
C = 0.000 ± 0.000
D = 1.0249 ± 0.0065
E = -1.0186 ± 0.0159
F = 0.290232 ± 0.029582
G = 1.00 ± 0.00

As it is clearly seen from fig.4.1 the relative efficiency of the detector is large for lower peak energies than for higher peak energies the due to larger the fact that the photoelectric cross-section at lower energies in Fig 1.6. The values of relative peak efficiency in fig.4.1 are not normalised to 100%, they only represent relative value of the efficiency. In general, the graph shows the behaviour of the efficiency of the detector in a wide energy range, which is a typical characteristics of most Ge detectors.

This efficiency curve leads to an error of about 2.5% in intensity measurement as compared to the true intensity of the source. The relative full-energy peak efficiency of the detector used here is 11% as compared with a 3" x 3" NaI(TI) scintillation detector.

4.2 ENERGY DEGRADATION

To irradiate different samples with various incident beam energy at a time use was made of the techniques commonly utilised for this purposes. This technique requires the preparation of different slices of the sample to be irradiated with appropriate size and weight. In our case, five slices from natural Ge crystal with various thickness were prepared. All the slices were packed together with thin aluminium foil, so that the slices were not allowed to make motion with respect to each other during irradiation. Fig.4.2 show how the package looks like.

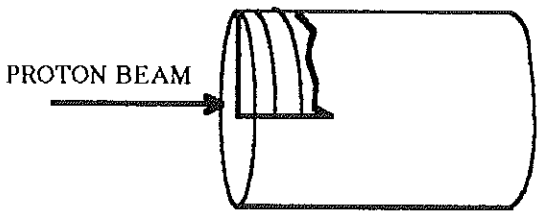

Fig.4.2 Ge crystals package with respect to the beam.

This package has been put on the target holder of the cyclotron, hence, during irradiation the incident beam first pass the aluminium foil crystal package before it hits the Ge crystals. Using a computer simulation programme called Transport of Ions in Matter (TRIM), calculations have been made to determine the incident energy on each slices of the crystal. The beam energy was set at 35 MeV for the first Ge crystal. As expected from the result of TRIM calculations, the incident proton beam energy degrades as it passes through the slices of Ge crystal targets. Therefore, each target slices are bombarded with different beam energy, and hence, it is this way that energy degradation was achieved.

4.3 DATA ON THE SAMPLES AND BEAM PROPERTIES

The circularly shaped samples were prepared with different thickness but nearly equal 10mm diameter. In this section data on the samples thickness and the result of TRIM calculation on the incident proton beam energies are given in table 4.2. Moreover, the following beam parameters were used during irradiation.

Proton beam current : 0.5μA

Diameter of the beam : 5.0 mm

Irradiation time : 10min.

Beam flux : 1.6 *10^{13} protons/cm^2 * sec

Table 4.2 The samples thickness and the corresponding incident energy from the result of TRIM calculation.

Sample Number	Thickness in (mm)	TRIM calculation for incident energy in (MeV)
Sample Nr.1	(0.74 +- 0.01)	35.00
Sample Nr.2	(0.72 +- 0.02)	(30.63 +- 0.15)
Sample Nr.3	(0.70 +- 0.01)	(25.82 +- 0.14)
Sample Nr.4	(0.67 +- 0.01)	(20.46 +- 0.14)
Sample Nr.5	(0.67 +- 0.02)	(14.02 +- 0.16)

4.4 IRRADIATION FACILITY

The samples to be studied in this work have been irradiated with a proton beam of the Karlsruhe Compact Cyclotron (KAZ), in Karlsruhe. Here a short description of the cyclotron used is presented.

The Karlsruhe Compact Cyclotron (KAZ)

To provide intense particle beams for different users, mainly from industry and medicine, the Karlsruhe Compact Cyclotron (KAZ) was established at the Forschungszentrum the Karlsruhe (KfK). The main parameters of the cyclotron are given in table 1.

Table 1

Main parameters of the Karlsruhe Compact Cyclotron (KAZ)

Accelerated particles ..... H^-

Beam energy ..... 15 - 42 MeV

Extracted beam current 200μA

Acceleration frequency ..... 26.8 MHz

High-freqency voltage ..... 30 kV

Number of magnet sectors 2

Diameter of the chamber ..... 120 cm

Mean magnetic field ..... 18.4 kG

Type of ion source ..... Penning

Beam extraction technique ..... Stripping

This cyclotron KAZ together with an relativistic isochroncyclotron (KIZ) can be used for different applications. Both accelerators are used in a dual-beam mode for materials research for nuclear fusion technologies.

The other main application with KAZ is activation of thin layers to determine the wear of the machine parts, where there is mechanical friction between them. This radiotracer technique for iron and non-iron metals is widely applied. The beam quality allows to obtain high homogeneity of the irradiated surfaces with depths of several 100μm. For these applications an external beam of high intensity is necessary. Beams larger than 200μA can be extracted with 100% efficiency. This result is reached with a special extraction technique. Ions of H^- are accelerated and then stripped on a thin carbon foil (see fig.4.3). Due to the different positions of two stripper foils isotope production and materials irradiation at different energies can be carried out at the same time without changing any of the accelerator parameters.

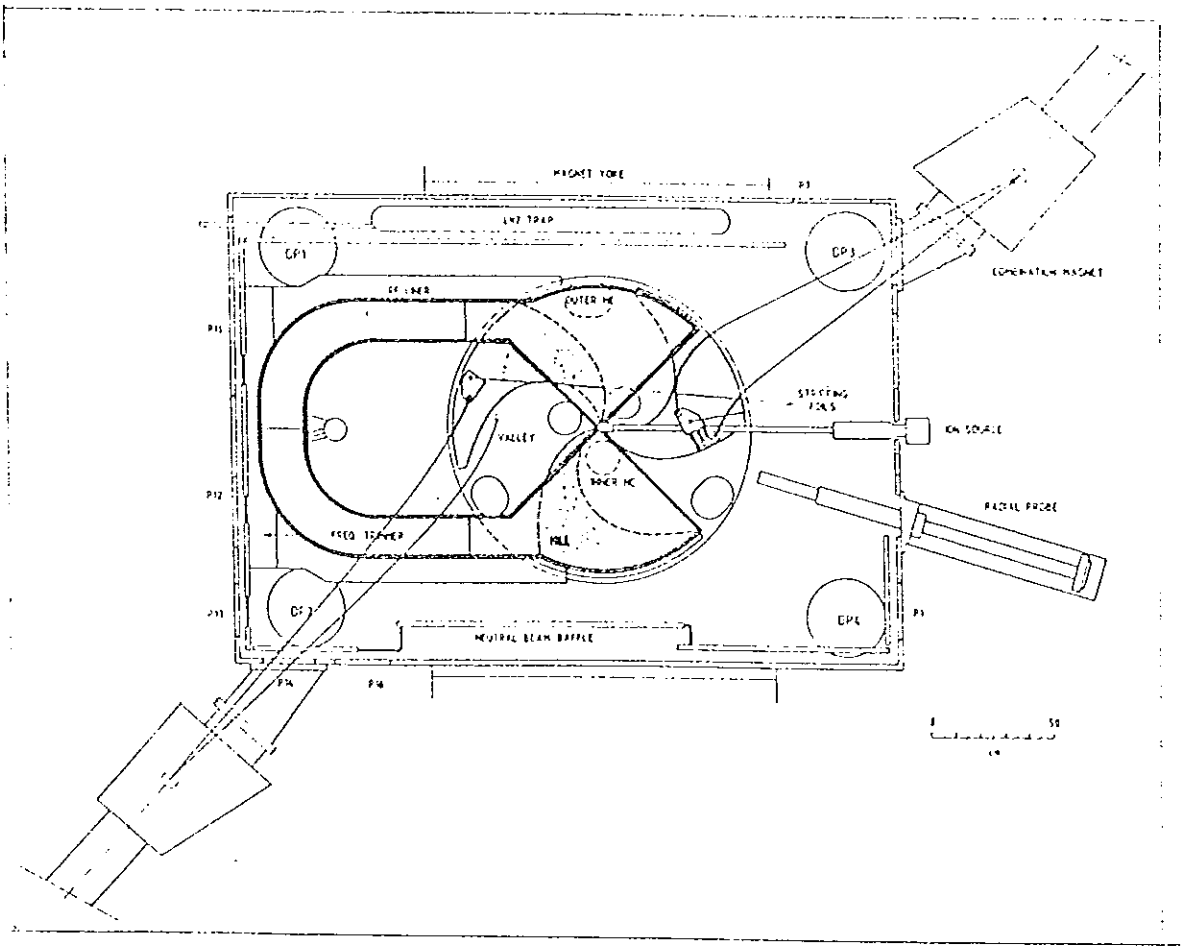

Fig.4.3 Schematic diagram of the KAZ cyclotron. The position of the stripper foils for 15 MeV and 35 MeV, and the beam trajectories are shown.

CHAPTER V

DATA ANALYSIS AND DISCUSSION

Introduction

As mentioned earlier in section 4.2, five slices of natural Ge-crystal samples have been irradiated. Spectral measurements were taken from each sample independently. The measurements were made for several times in different time intervals. The time intervals were ranging from 20 minutes on the day when the measurement was started, and to 90 minutes on the last day of the measurement. All measurements were taken at the source-detector distance of 4.2cm. At the beginning, the activity from each irradiated samples was so high that the dead time of the detector was too long. Therefore, it was necessary to wait for some days until the activity became convenient for measurement.

In the spectra seven isotopes were identified, of which six of them were found in all the samples, and one short lived isotope was observed in the first and the second samples. Therefore, analysis have been carried out only on those isotopes which were observed in all the samples. The seventh isotope ^{68}Ga was short lived ($T_{1/2}$= 68.3 min) and even the information obtained was not even sufficient to carry out further analysis.

To avoid the effect of γ-ray incident angle on the detector because of the geometry conditions of the samples, the samples were positioned one after another on one face of a lead brick, and the brick was placed in front of the detector for spectral measurement. However, radiation from the samples cause some fluorescent X-rays of lead like (75 keV and 85 keV) lines and the K-edge of lead at energy (88 keV), these X-rays were also detected. These X-ray lines are seen at low energy region of the spectrum. Hence the lines are identified not to be confused with those lines from the irradiated samples. Besides, every time before measurements were started from the samples, the background of the room was measured. In all the background spectra (appendix C), a peak with energy 1460 keV was

observed. This line appears because of ^{40}K, which was always present in the walls of the laboratory room and the surrounding. Finally, at 511keV line some annihilation lines from different β^+ emitters overlap, hence this lines can not be used for quantitative nuclide analysis.

5.1 MEASURED SPECTRA AND OBSERVED RADIOACTIVE ISOTOPES.

The spectra shown in fig.5.1(a) up to fig.5.1(e) are the spectra taken from each sample, 216 hours after irradiation. From the measured spectra the isotopes ^{67}Ga, ^{69}Ge, ^{71}As, ^{72}As, ^{74}As, and ^{76}As are observed in all the samples. The isotopes ^{73}As and ^{75}As must be among the expected reaction products. But, the isotope ^{75}As is stable and therefore can not be detected in this measurement. Moreover, ^{73}As is a long lived radioactive isotope with half life of 80.3d, it emits two very low energy γ- rays (13.27 keV and 53.44 keV), which were below the threshold of the measurement and therefore do not appear in the spectra. The background stripping was not carried out in our measurement because, the activities of the source were so strong that all the major decay lines of the isotopes were seen above the background spectrum.

Here we present the first half of the spectra taken from each sample, which contains all major decay lines of the observed isotopes. The second half of the spectra are given in appendix B. In the spectra the centroid peak energies are given, these energies should be read in plus and minus between the values (1 to 1.5) keV. The major decay lines of the observed isotopes used to calculate the yield of the corresponding isotopes are marked with the corresponding transition probabilities. Similarly, the sample numbers refers to the corresponding incident energy as shown in table 4.2. Most of the main lines of the isotopes are identified in the spectra, those strong lines which are used to identify the elements are seen in repetitive measurement.

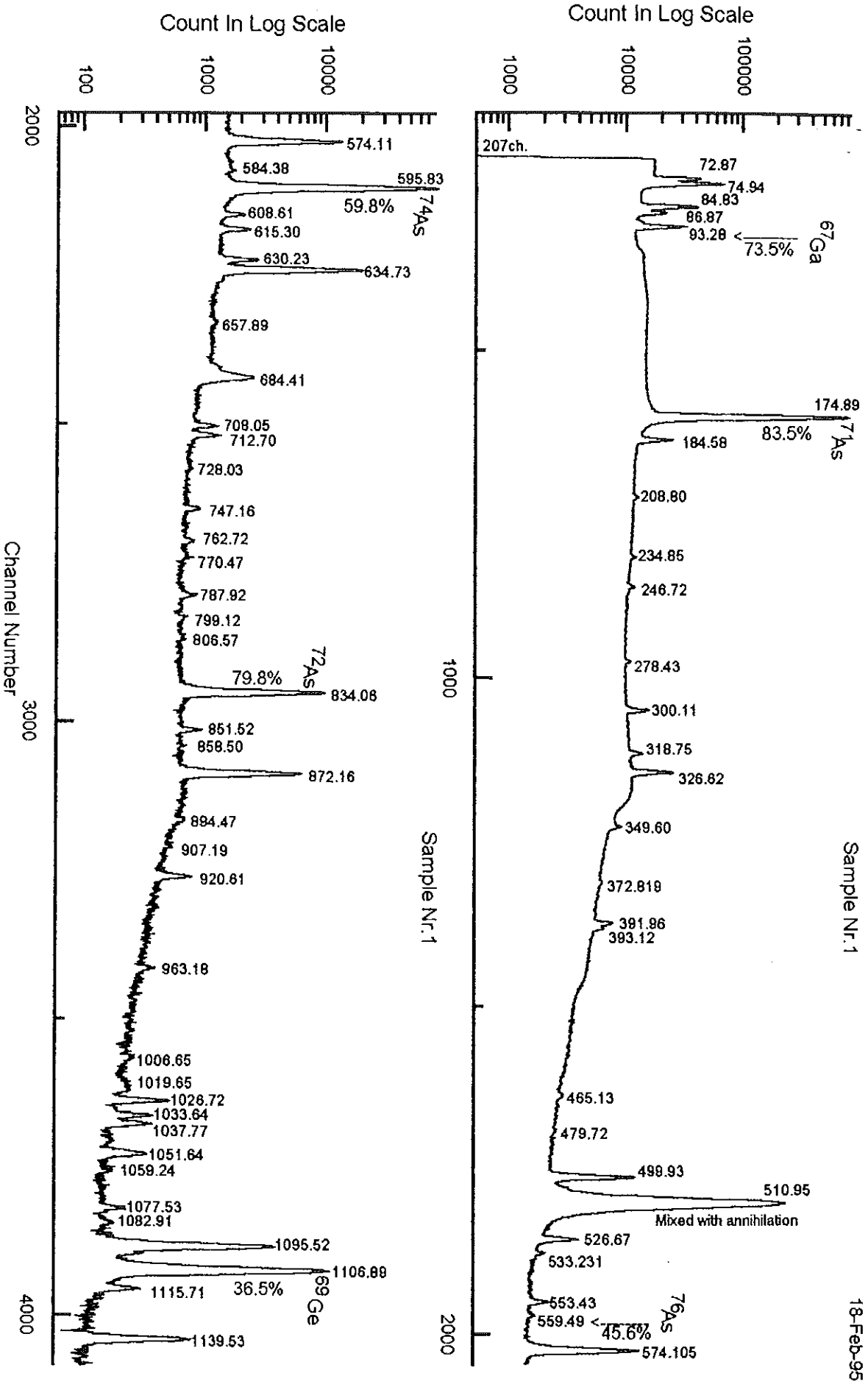

Fig.5.1(a) The first half of the spectrum from sample Nr.1

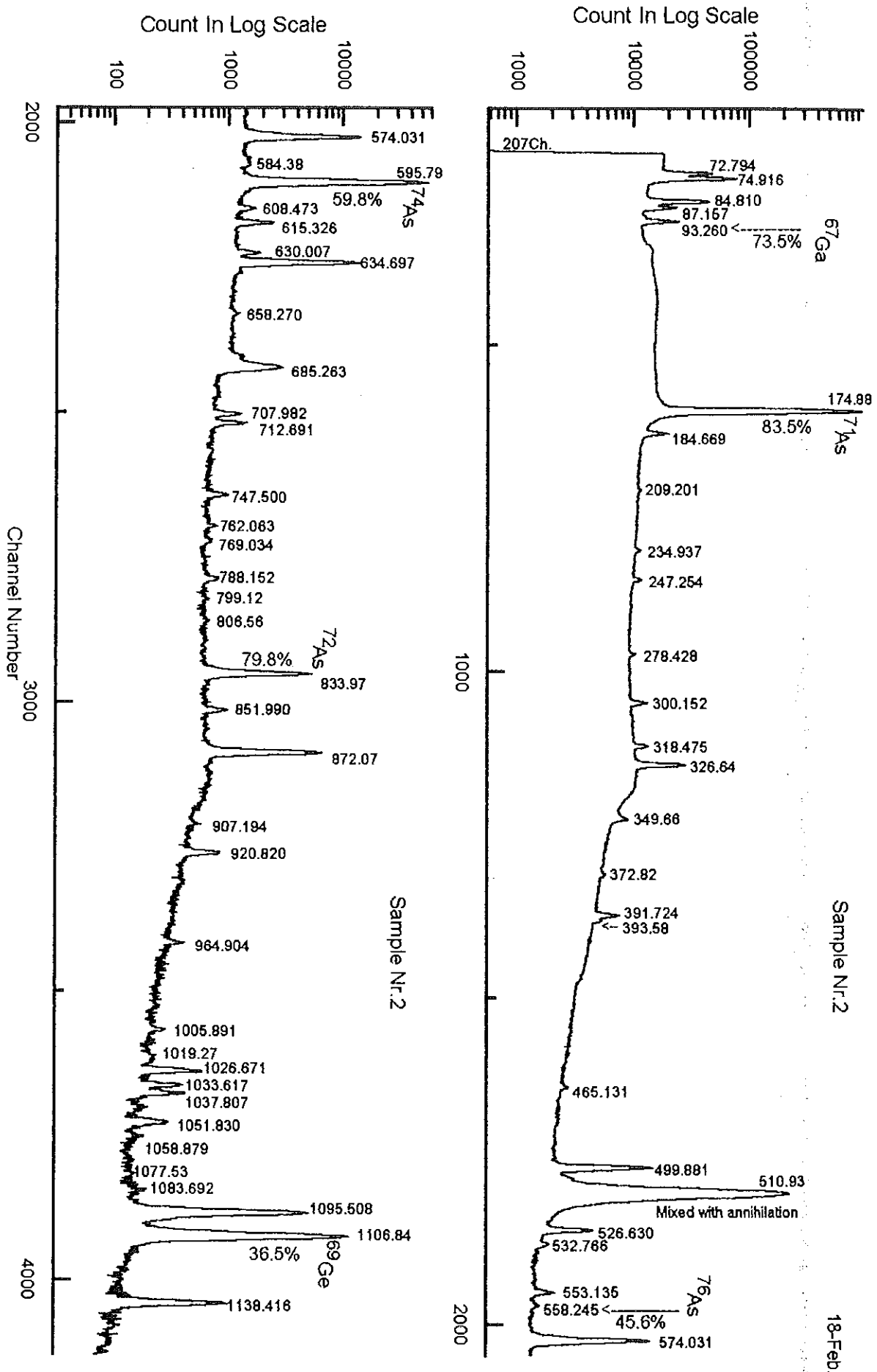

Fig.5.1(b) The first half of the spectrum from sample Nr.2

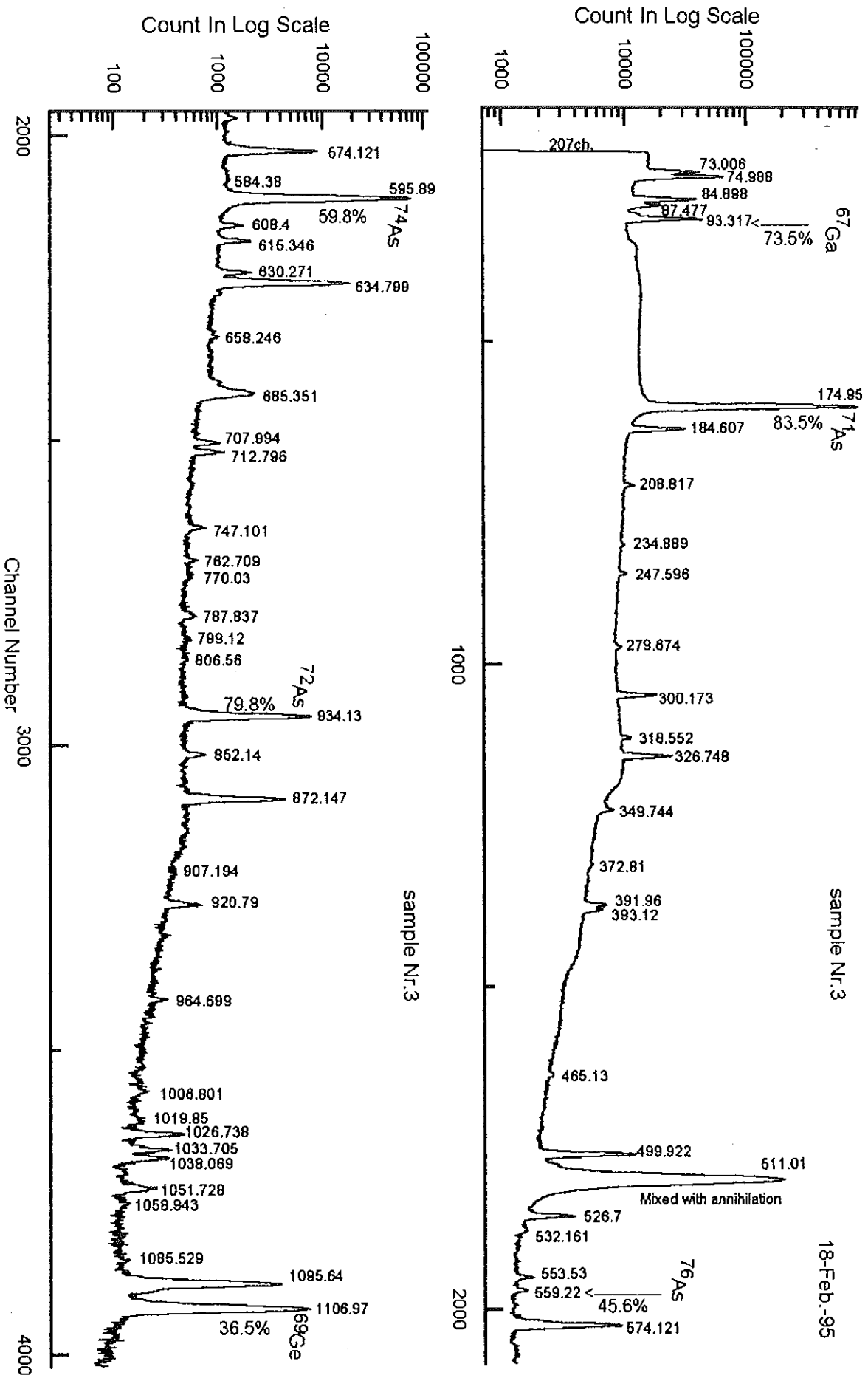

Fig.5.1(c) The first half of the spectrum from sample Nr.3

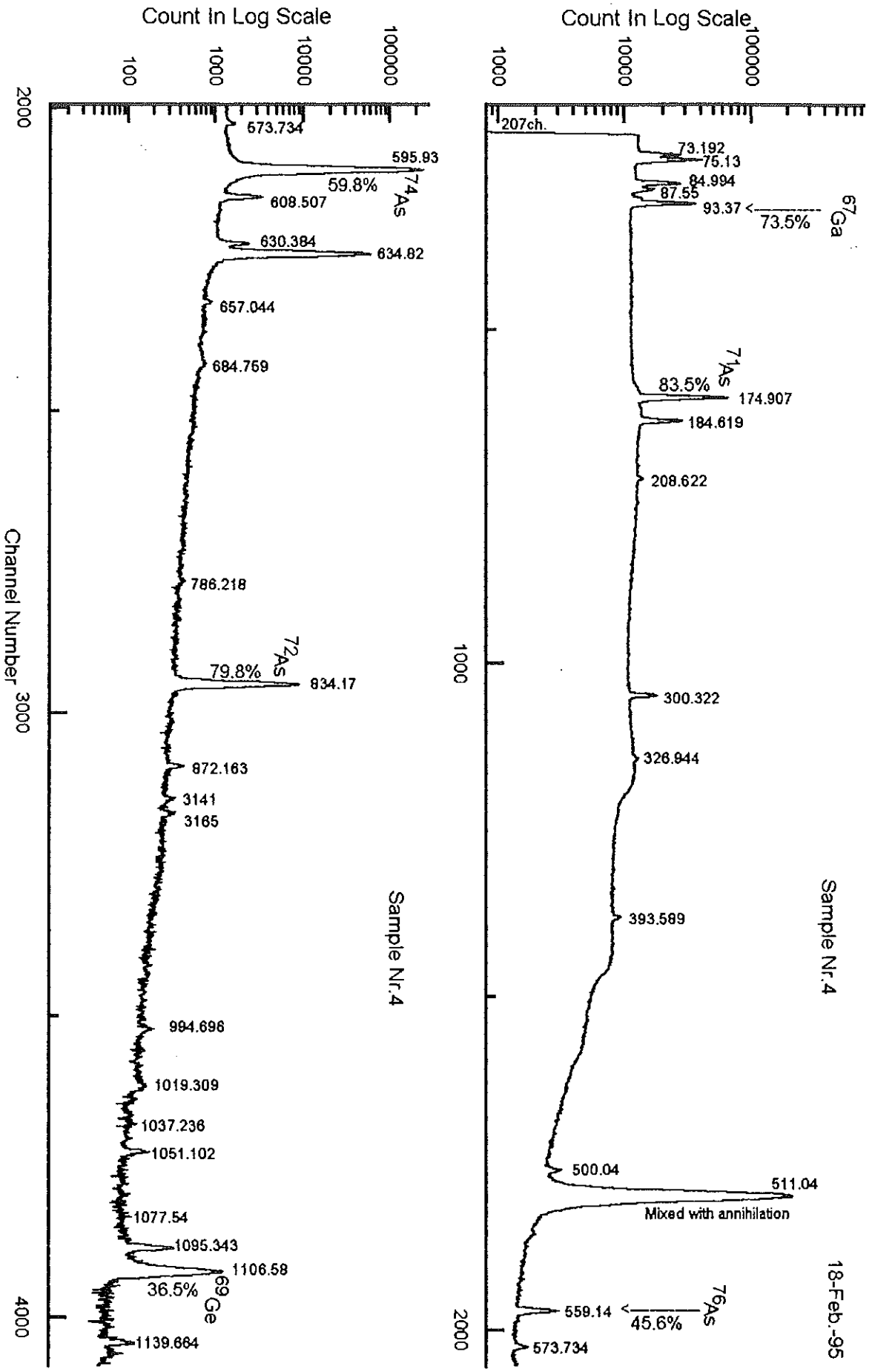

Fig.5.1(d) The first half of the spectrum from sample Nr.4

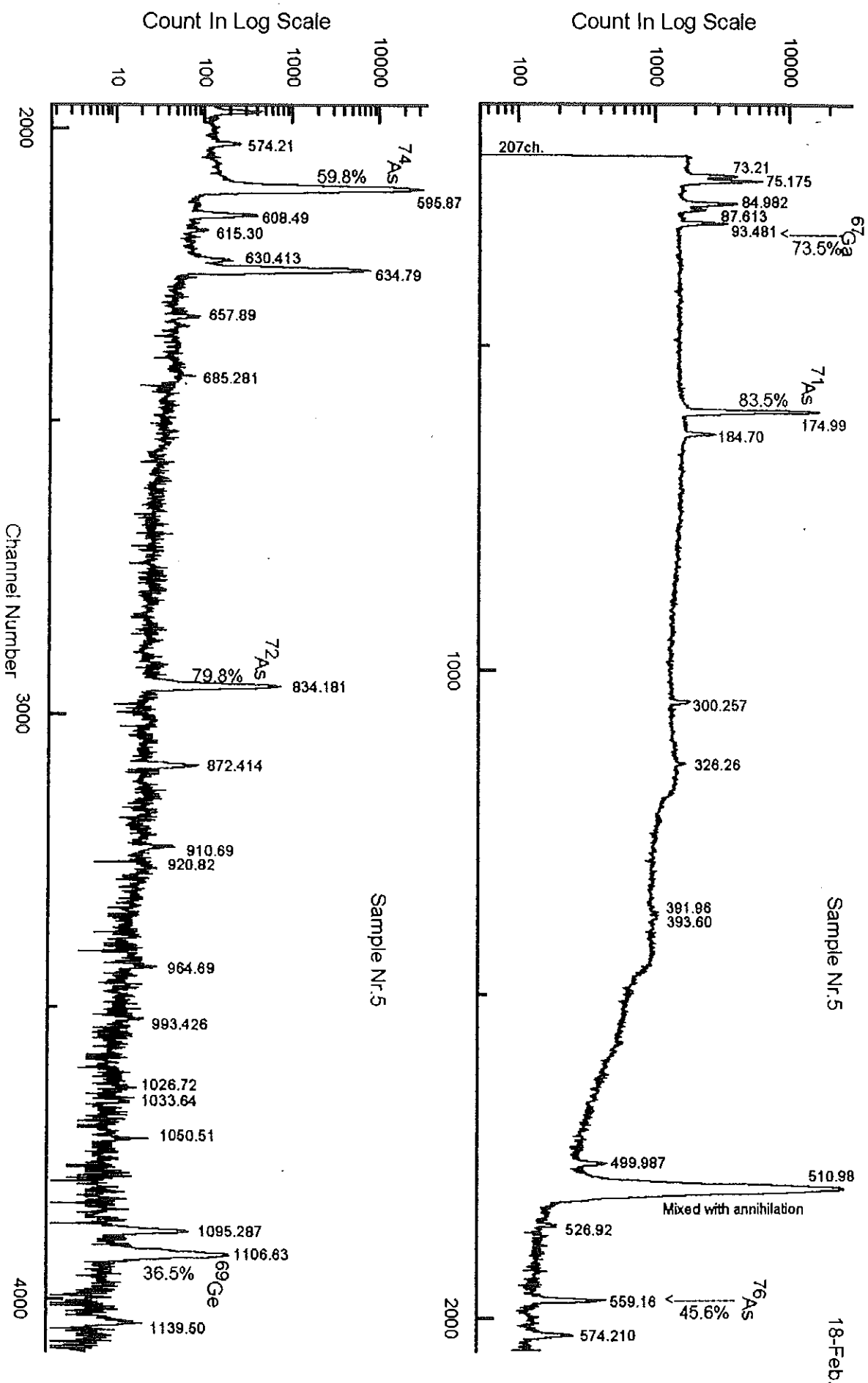

Fig.5.1(e) The first half of the spectrum from sample Nr.5

5.2 ISOTOPE YIELDS

After the isotopes were identified a major decay line of each isotope was selected, and the net peak area of the major decay line of each isotope is corrected by the efficiency of the detector, to obtain the true intensities of the γ-emitter. Then extrapolation were carried out to 100% of the nuclei created. In the calculation for the activity of the isotopes, use has been made from activity calibrated source ^{54}Mn which emits 835 keV γ-ray line with 100% transition probability. In other words, measurements are taken for equal time interval and at the same distance from the detector, for each sample and for the activity calibrated source ^{54}Mn independently. Using the measured intensities from the major decay lines of every isotopes, the corresponding activities were calculated by comparing them with the measured intensity of ^{54}Mn. The remaining calculations were simple application of the exponential decay law to take into account the delay time after irradiation. The calculation scheme for obtaining yield of the isotopes is given in (fig.5.2).

The isotopic yields obtained from the result of these calculations are given in fig.5.3. Among all the samples, the sample irradiated with 14.02 MeV energy yields one order less than the other samples (refer fig.5.3). Moreover, with the chosen energy region of interest, different incident energy produces different yields of arsenic isotopes. According to the result of the measurement seen in fig.5.3, maximum yields of ^{72}As, ^{74}As and ^{76}As are obtained at an incident energy of 20.46 MeV. Similarly, high yields of ^{71}As is obtained at 30.64MeV incident energy. On the contrary, the yield of ^{69}Ge increases continuously with energy. The maximum yield of ^{67}Ga is found at an energy of 25.82 MeV.

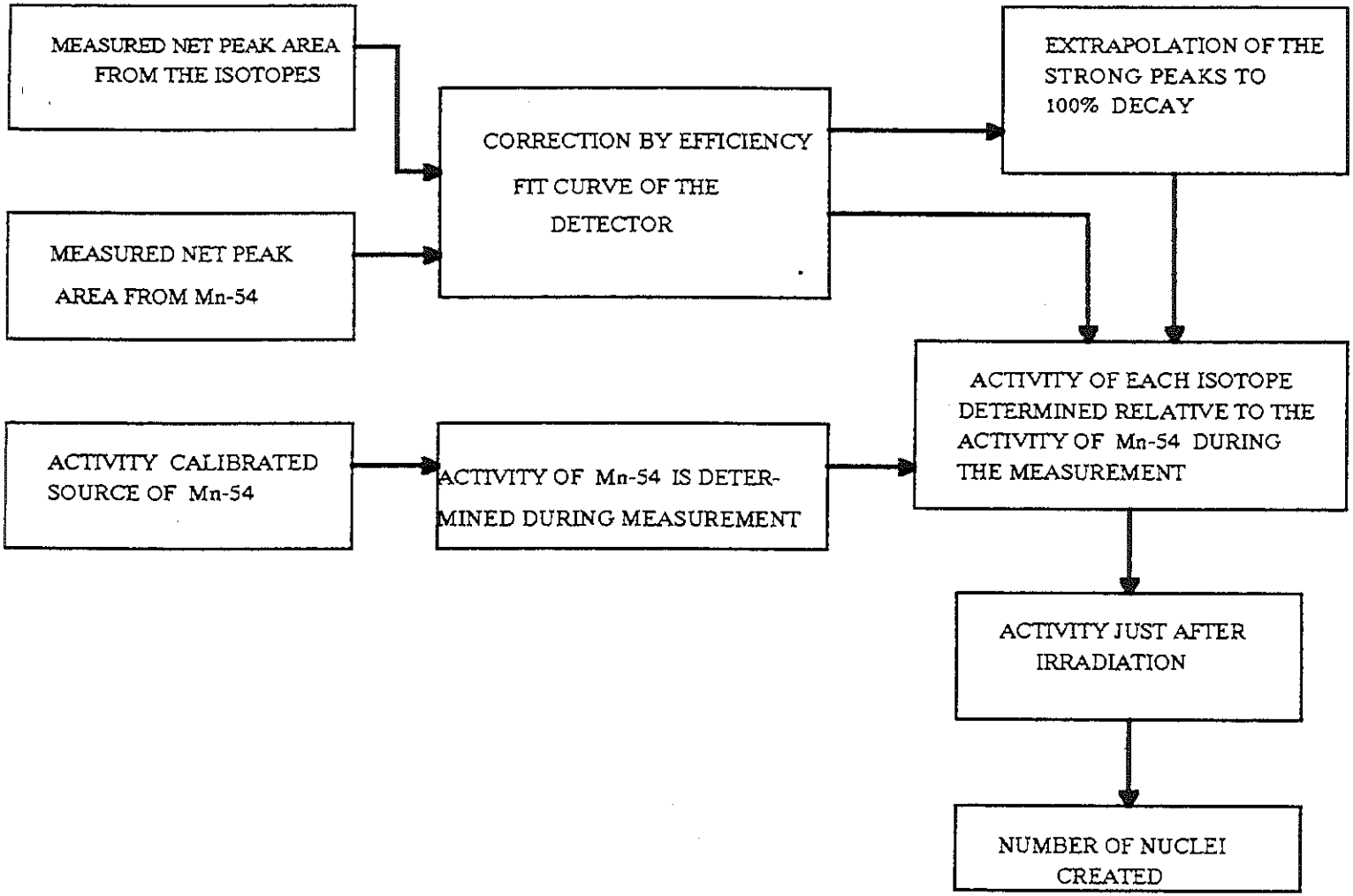

Fig.5.2 Layout of the calculation made for the yield of radioactive isotopes

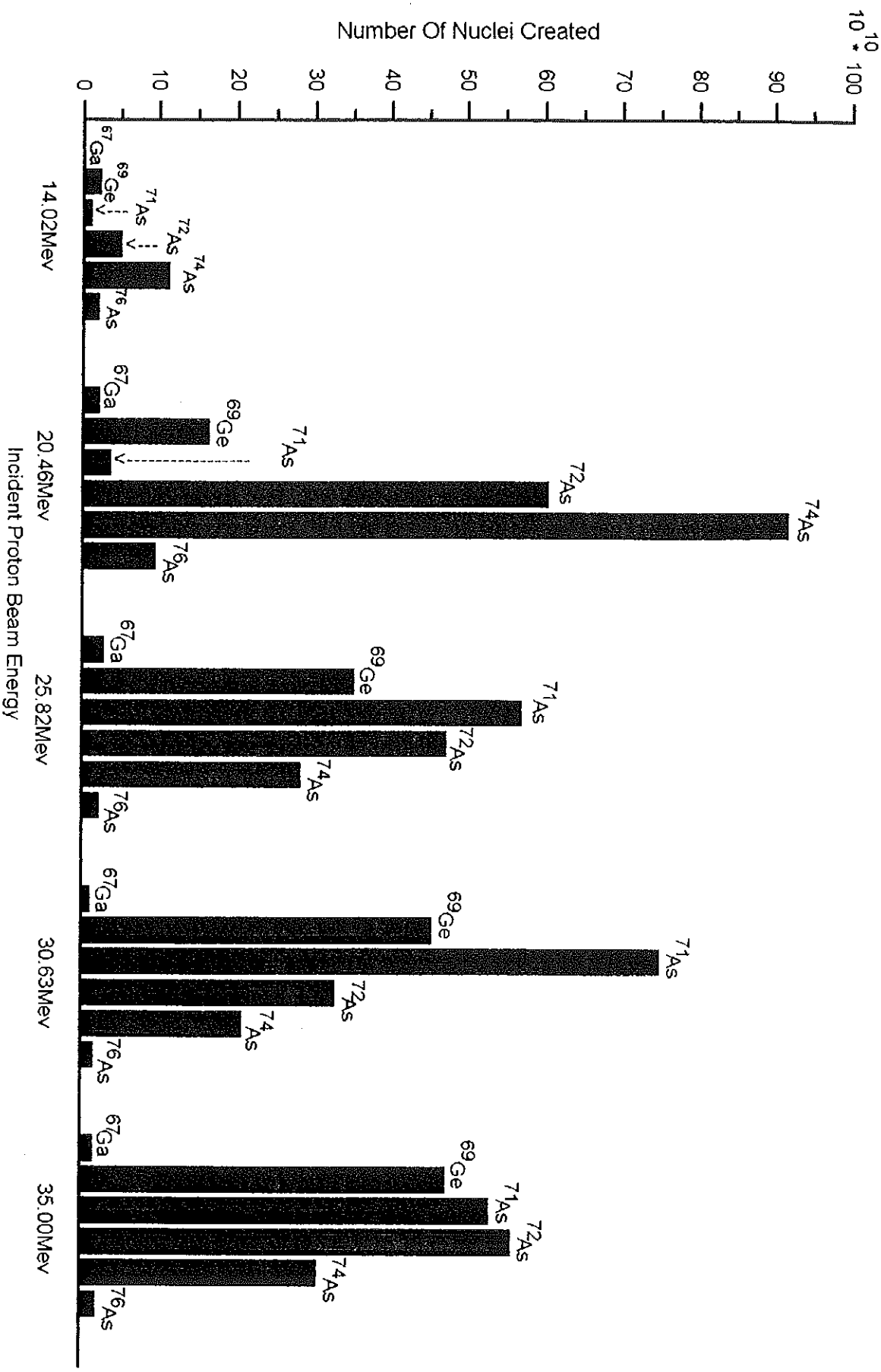

Fig.5.3 Isotopic yield in the samples. In the diagram the horizontal axis represent incident proton beam energies, with which the corresponding slice is irradiated.

5.3 POSSIBLE TYPES OF REACTIONS AND DECAY SCHEMES FOR THE ISOTOPES

The natural germanium crystal targets used are composed of the isotopes ^{70}Ge, ^{72}Ge, ^{73}Ge, ^{74}Ge and ^{76}Ge, with different abundance as given in table 5.1. Our expectation from the outcome of irradiating Ge-crystal by proton beam, in a chosen energy region of interest, was to produce arsenic isotopes. During irradiation a germanium nucleus captures a proton resulting in the formation of a compound nucleus. The proton embedded in the target nucleus transfers energy to the neighboring nucleons, and as a consequence some of the neutrons are evaporated, in such a way that different arsenic isotopes are created. This process is followed by β^+ or β^- decay or electron capture processes together with gamma ray emission until stable elements are attained. Moreover, the following decays are known to be followed by the reaction produets of As isotopes.

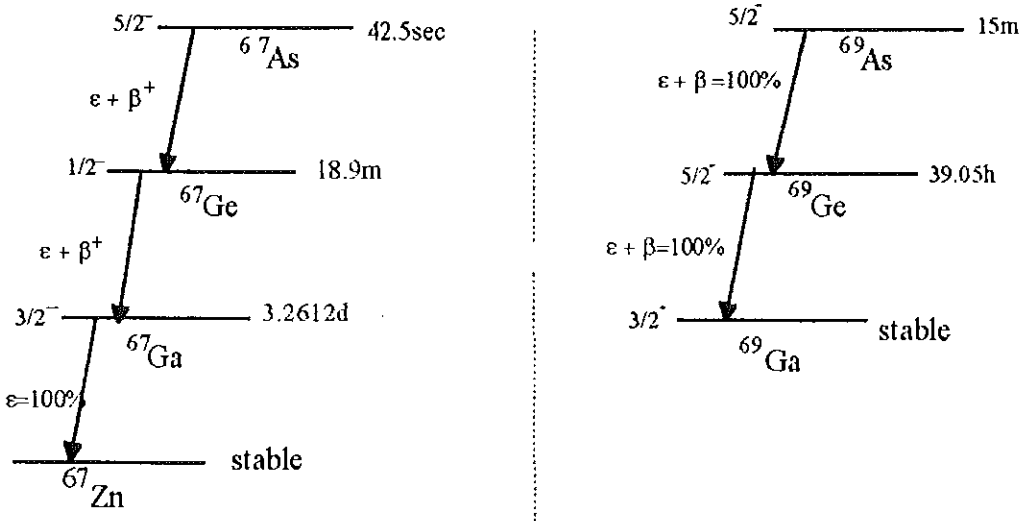

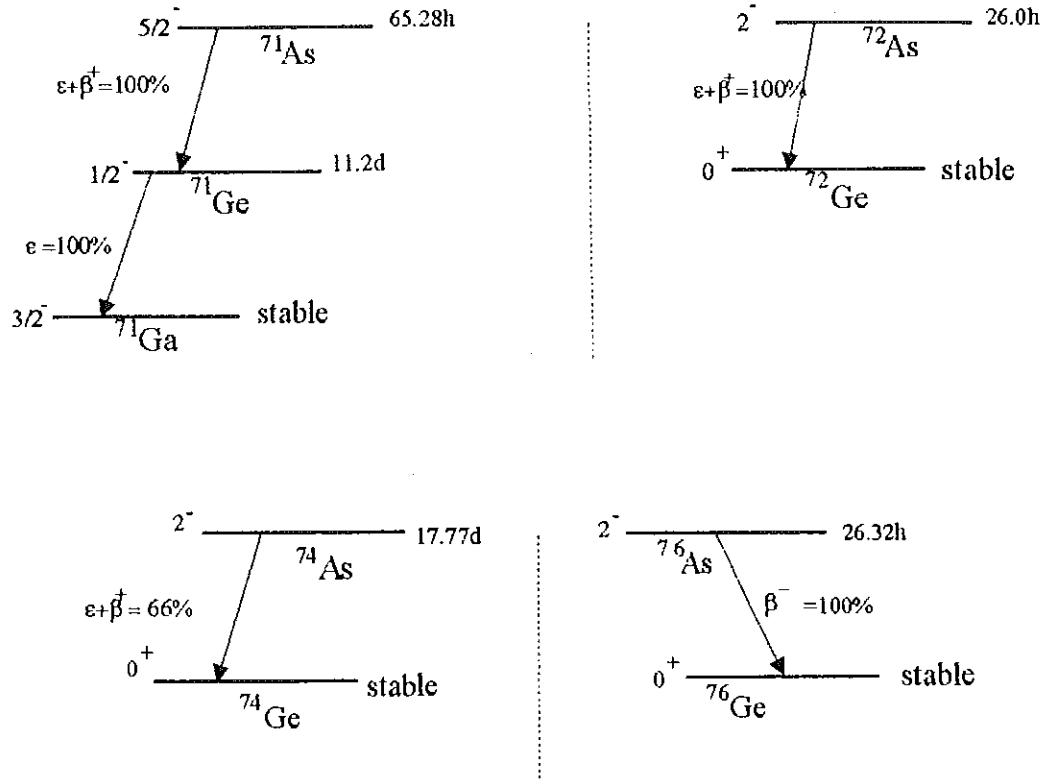

Fig.5.5 Decay schemes of the observed isotopes

According to the result of the experiment the prominent nuclear reactions are the (p,n) charge exchange and (p,xn) neutron evaporation reactions, to produce As nuclides. The possible types of reactions leading to the creation of As nuclides are tabulated in tab.5.1

Table 5.1 The possible types of reactions and abundance of Ge isotopes in the target

Reaction product	Possible types of reactions	Abundance of Ge isotopes in the targets
^{67}Ga	^{70}Ge (p,4n)^{67}As	
^{69}Ge	^{70}Ge (p,2n)^{69}As ^{70}Ge (p,d)^{69}Ge ^{72}Ge (p,4n)^{69}As	^{70}Ge ----------> 20.7%
^{71}As	^{72}Ge (p,2n)^{71}As ^{73}Ge (p,3n)^{71}As ^{74}Ge (p,4n)^{71}As	^{72}Ge ---------> 27.5% ^{73}Ge ---------> 7.7% ^{74}Ge ----------> 36.4%
^{72}As	^{72}Ge (p,n)^{72}As ^{73}Ge (p,2n)^{72}As ^{74}Ge (p,3n)^{72}As	
^{74}As	^{74}Ge (p,n)^{74}As ^{76}Ge (p,3n)^{74}As	^{76}Ge ---------> 7.7%
^{76}As	^{76}Ge (p,n)^{76}As	

5.4 REACTION CROSS-SECTIONS

Use has been made from relation 3.8 for calculating the reaction cross-section of the observed reaction products. In these calculations the activity of the observed isotopes are involved, but this activity was obtained as the result of all the possible reactions occurrence leading to the production of a given isotope. Hence, it is impossible to distinguish exactly how much was the contribution for measured activity from a given reaction type in this measurement. Therefore, we used the measured activity from a reaction product in the relation 3.8 for calculating the cross-section. Because, it is required here only to obtain information on the value of maximum probability of occurrence for a given reaction product, from natural germanium target. Eventhough use is made from the measured activity for the cross-sections, inorder to apply equation 3.8 use is made of one of the possible reaction for the production of a given product.

According to the result of the calculations for reaction cross-sections, shown in fig.5.6, except the reaction cross-section for the production of ^{69}Ge which increases continuously with energy, all of them attain a maximum value of the cross-section in the energy region of interest. These results are given in table 5.2.

Table 5.2 Maximum reaction cross-section for the observed reaction products

Reaction product	Incident energy for maximum yield (MeV)	Maximum Cross-section (mb)	Threshold energy (MeV)
^{71}As	30.63	464	13.5 +- 1.5
^{72}As	20.46	403	13.2 +- 1.2
^{74}As	20.46	474	12.7 +- 1.2
^{76}As	20.46	239	12.5 +- 1.2
^{69}Ge	----	----	12.6 +- 2.0
^{67}Ga	25.82	24	----

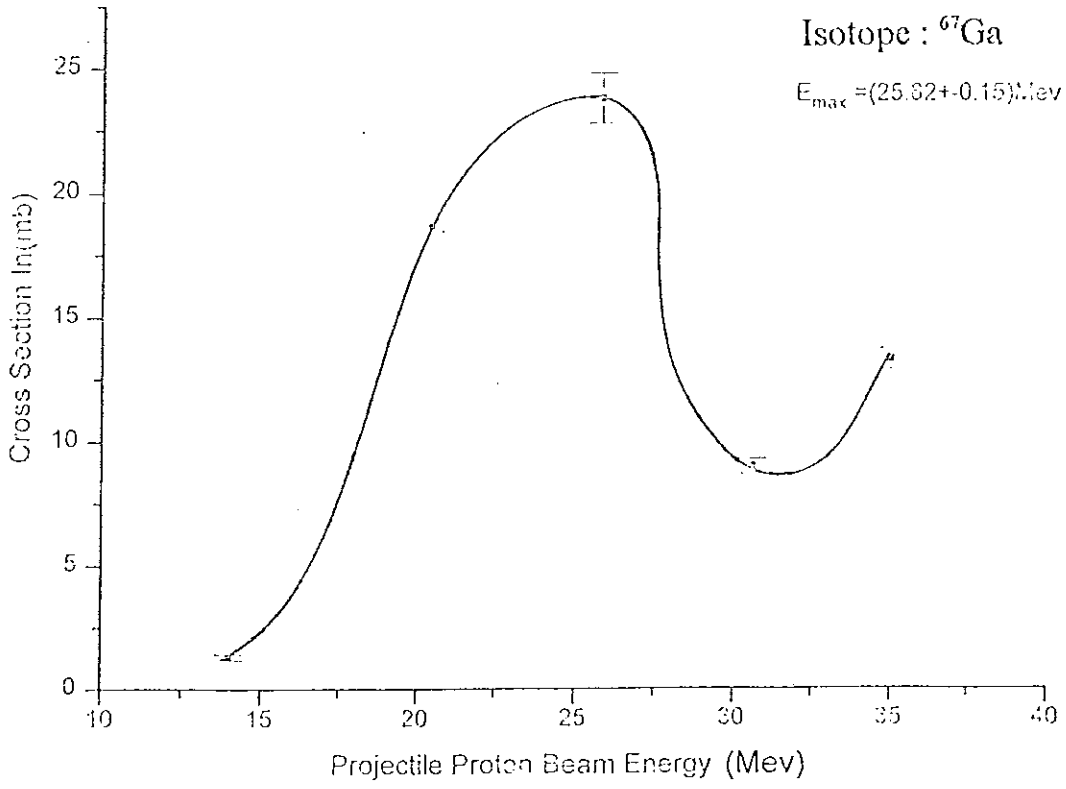

Fig.5.6(a) Reaction cross-section for production of ^{67}Ga from natural Ge target

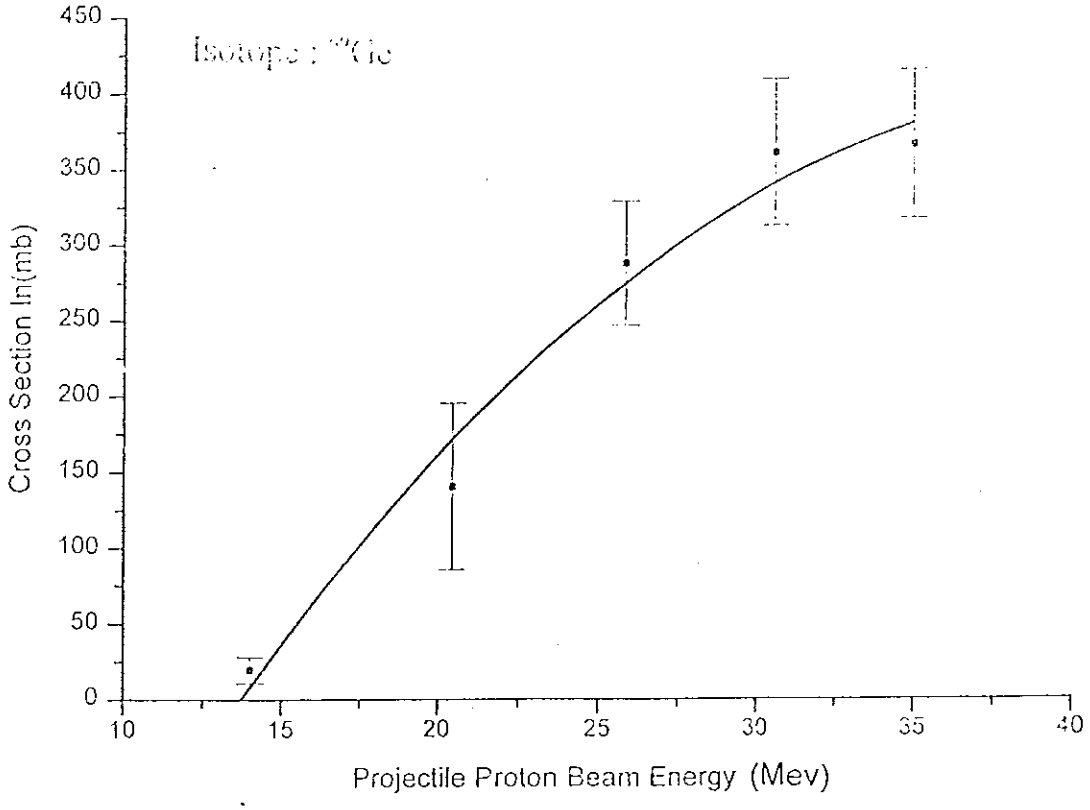

Fig.5.6(b) Reaction cross-section for production of ^{69}Ge from natural Ge target

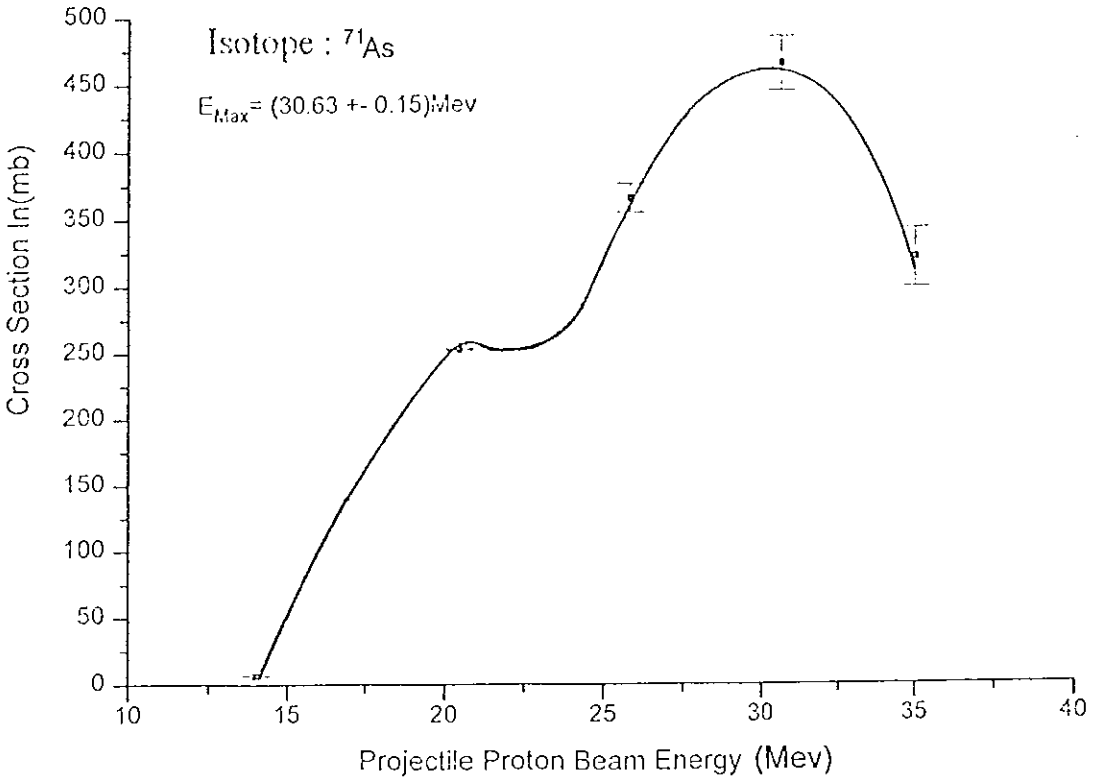

Fig.5.6(c) Reaction cross-section for production of ^{71}As from natural Ge target

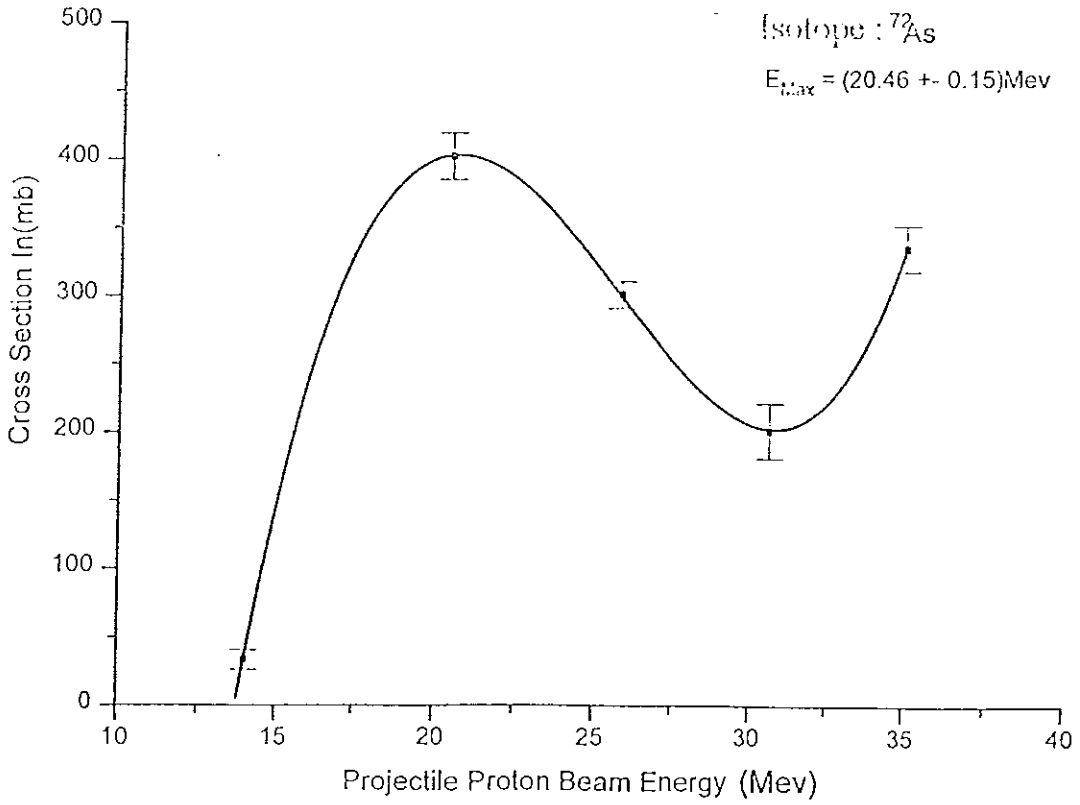

Fig.5.6(d) Reaction cross-section for production of ^{72}As from natural Ge target

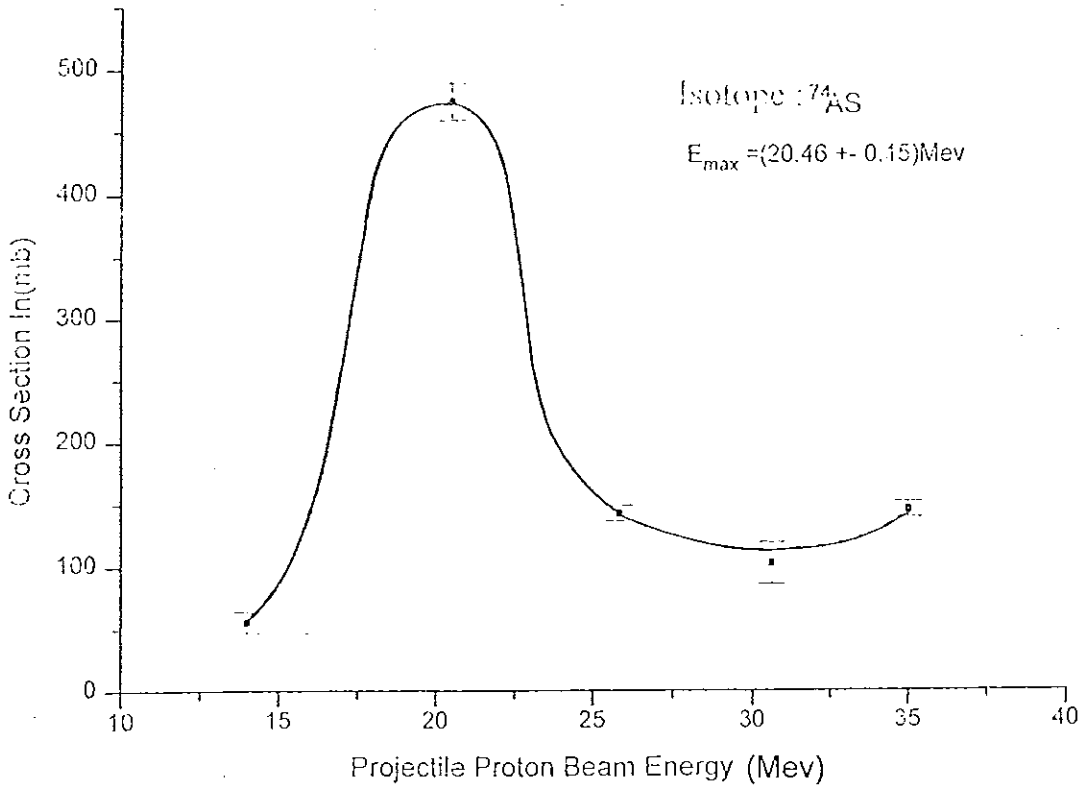

Fig.5.6(e) Reaction cross-section for production of ^{74}As from natural Ge target

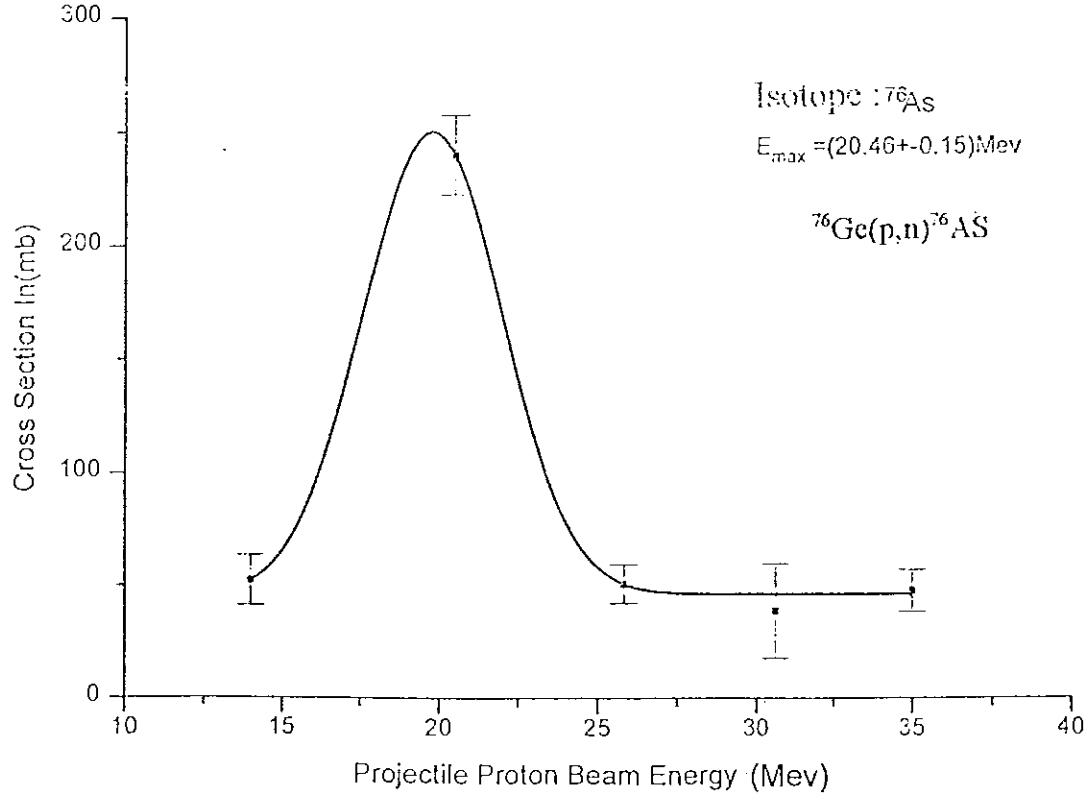

Fig.5.6(f) Reaction cross-section for production of ^{76}As from natural Ge target

Among all the possible types of reaction listed in table 5.1 the cross-sections for the reaction of the type (p,n) and (p,2n) were more expected in this experiment than to the cross-section of the type (p,4n) reaction in a given energy region. The (p,4n) reaction is introduced here because of ^{67}Ga, which was observed in all the samples. Besides, the threshold energies are obtained by extrapolation from fig.5.6. On the other hand, the magnitude of the cross-section for the production of ^{76}As is relatively smaller than the other calculated value of the cross-sections. This is due to the lower abundance of ^{76}Ge isotope in natural germanium crystal target (see table 5.1). In contrast to this, the maximum value of the cross-section for ^{74}As is accounted to the high abundance of ^{74}Ge isotopes in the target through ^{74}Ge(p,n)^{74}As reaction.

We compare next the magnitude of the calculated reaction cross-sections and the results obtained from similar reactions using gallium target (ref.9). We present in table 5.3 the maximum values of the reaction cross-section for some selected reaction types. These values are taken within the same energy region chosen for the reaction.

Table 5.3 Maximum reaction cross-section for gallium (from ref.9)

Reaction	Cross-section (mb)	Incident energy for the maximum yield (MeV)
^{71}Ga(p,3n)^{69}Ge	485	31
^{71}Ga(p,4n)^{68}Ge	146	>31
^{69}Ga(p,pn)^{68}Ga	345	24.5

For the reason that we lack values of reaction cross-sections for the germanium target from other experiments, here gallium is selected because its mass number is comparable with that of germanium isotopes. From this comparison we believe that the calculated values of the cross-sections are reasonable for the observed reactions.

In general the energy dependence of the reaction cross-sections varies with the type of reactions in a wide energy range (as seen in ref.9). In this work also we have obtained varied shapes of the cross-sections with energy for the observed reactions. In fact, use have been made of natural Ge-target which is composed from many germanium isotopes, that opens different reaction channels for a given reaction product. This accounts for the different shapes of the cross-sections.

CONCLUSION

In the spectra of the irradiated samples, all the isotopes discussed in the data analysis part are observed in reliable degree of confidence. Among all the possible types of reactions listed in table 5.1, it was less expected to have the (p,4n) reaction in the chosen energy range. But, because of the existence of isotope ^{67}Ga in all the irradiated samples, we introduce (p,4n) reaction to incorporate it in the discussion, but it becomes unclear why this reaction is observed to an incident energy down to 14MeV. Moreover, by the very nature of the target used most of the calculated reaction cross-sections did not represent a single reaction type but a mixture of all the possible reactions leading to the production of a given reaction product. The only clean reaction cross-section we have in this experiment is the cross-section for the production of ^{76}As from the reaction ^{76}Ge(p,n)^{76}As.

Regarding the yields of the isotopes, and the result of the calculation for reaction cross-sections, high value of the cross-sections are obtained for isotopes ^{72}As, ^{74}As, and ^{76}As at an incident energy of 20.46 MeV. The isotope ^{71}As has high cross-section at an energy of 30.63MeV. Besides, a better yields of ^{67}As is observed at an incident energy of 25.82MeV, but the magnitude of its cross-section is very low as compared to the cross-sections of the other isotopes. Finally, the calculated values of the reaction cross-sections are found to be quiet reasonable as compared to the reaction cross-sections of gallium isotopes taken from ref.9.

REFERENCES

1. N.R.Leo, Techniques for nuclear and particle physics experiments, Springer-Verlag, 1994.
2. F.Knoll, Radiation detection and measurement, John Wiley & Sons, New York, 1988.
3. H.Ryssel and I.Ruge, Ion Implantation, John Wiley & Sons Ltd, Toronto, 1986.
4. G.Carter, Ion Implantation of Semiconductors, Edward Arnold Ltd, London, 1976.
5. Landolt-Börnstein, Numerical Data and Functional Relationships in Science and Technology, Volume 5, Berlin, 1973.
6. W.S.C. Williams, Nuclear and particle physics, Oxford, 1991.
7. G.Miller and Dudley, Radioactivity and radiation detection, New York, 1972.
8. W.Marth, Irradiation technique at research reactor, Germany, 1969.
9. J.B.Marion and F.C.Young, Nuclear reaction analysis, North-Holland, 1968.
10. J.L. Putman and W.J.Whitehouse, Radioactive Isotope, Oxford University Press, London, 1953.
11. Nuclear Data Sheet, Volume 42, Academic press, Inc. 1984.
12. Nuclear Data Sheet, Volume 51, Academic press, Inc. 1987.
13. Nuclear Data Sheet, Volume 53, Academic press, Inc. 1988.
14 Nuclear Data Sheet, Volume 55, Academic press, Inc. 1989.
15. Nuclear Data Sheet, Volume 56, Academic press, Inc. 1989.
16. Nuclear Data Sheet, Volume 58, Academic press, Inc. 1989.
17. Nuclear Data Sheet, Volume 64, Academic press, Inc. 1991.
18. P.N.Cooper, Introduction to nuclear radiation detectors, Cambridge University Press, London, 1986.
19. Edgado Brown, Tables of isotopes, Wiley-Interscience Publication, New York, 1978.

20. M.Stanley Livingston, High-energy accelerators, Interscience Publishers, Inc., New York, 1954.

21. David K.Brice, Ion implantation range and energy deposition distributions, Volume 1. NewYork 1975.

22. Th.Schaefer, M.Wehner, K.Freitag and R.Vianden, Donor-Defect Interaction in Semiconductors, a report to the Physics school of Bonn University, Bonn, 1994.

23. K.N.Mukhin. Experimental Nuclear Physics. Volume 1, Mir. publishers, Moscow. 1987.

24. D.C.Radford, EFFIT software, "Workshop on Large γ-ray Detectors Arrays". Chalk River Laboratories, 1992.

25. J.F.Ziegler, J.P.Biersack and U.Littmark, Transport of Ions in Matter, Pergamon press. New York, 1985.

26. Bernared G. Harvey, Introduction to Nuclear Physics and Chemistry, Prentice-Hall. Inc., New Jersey, 1969.

27. E.U.Condon and Hugh Odishaw, Handbook of Physics, McGraw-Hill. New York, 1967.

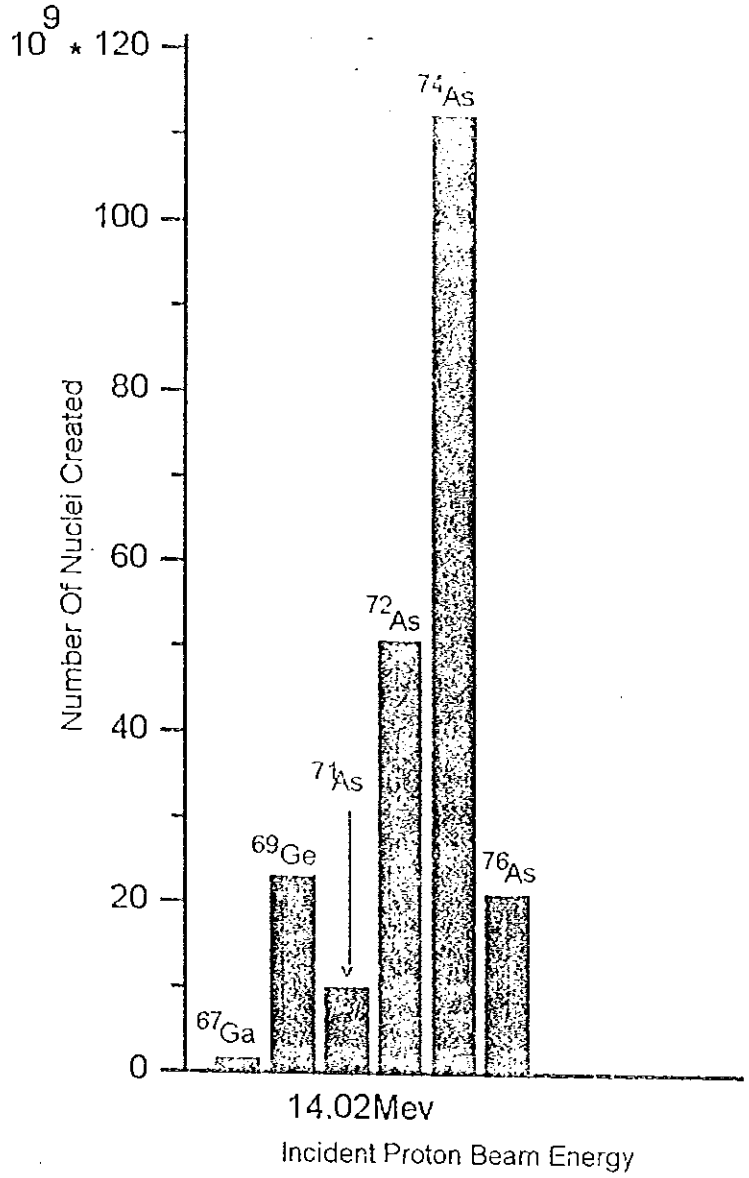

Appendix A. An enlarged view of isotope yield of the sample irradiated with 14.02MeV proton beam

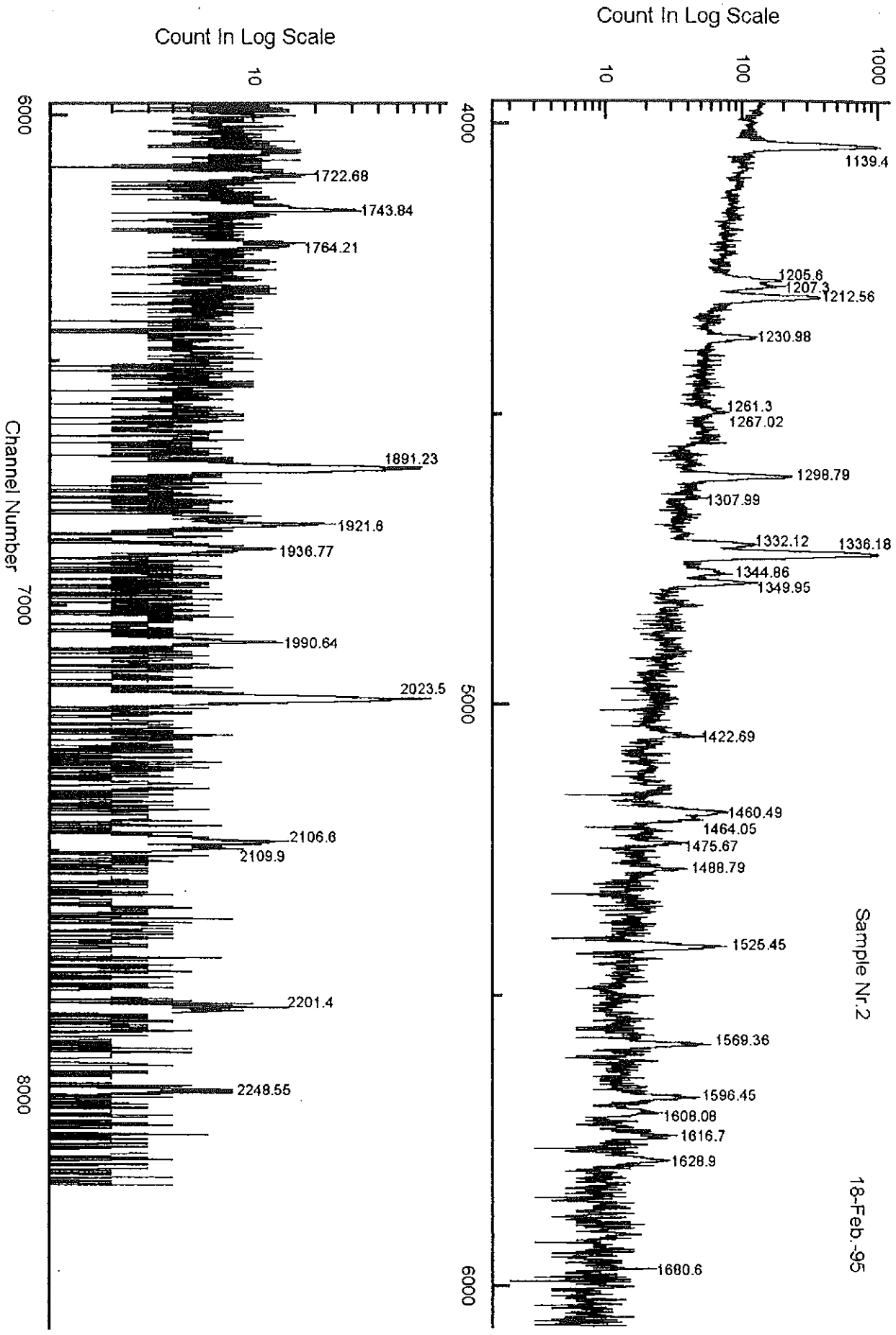

Fig.B.2 The second half of the spectrum from sample Nr.2

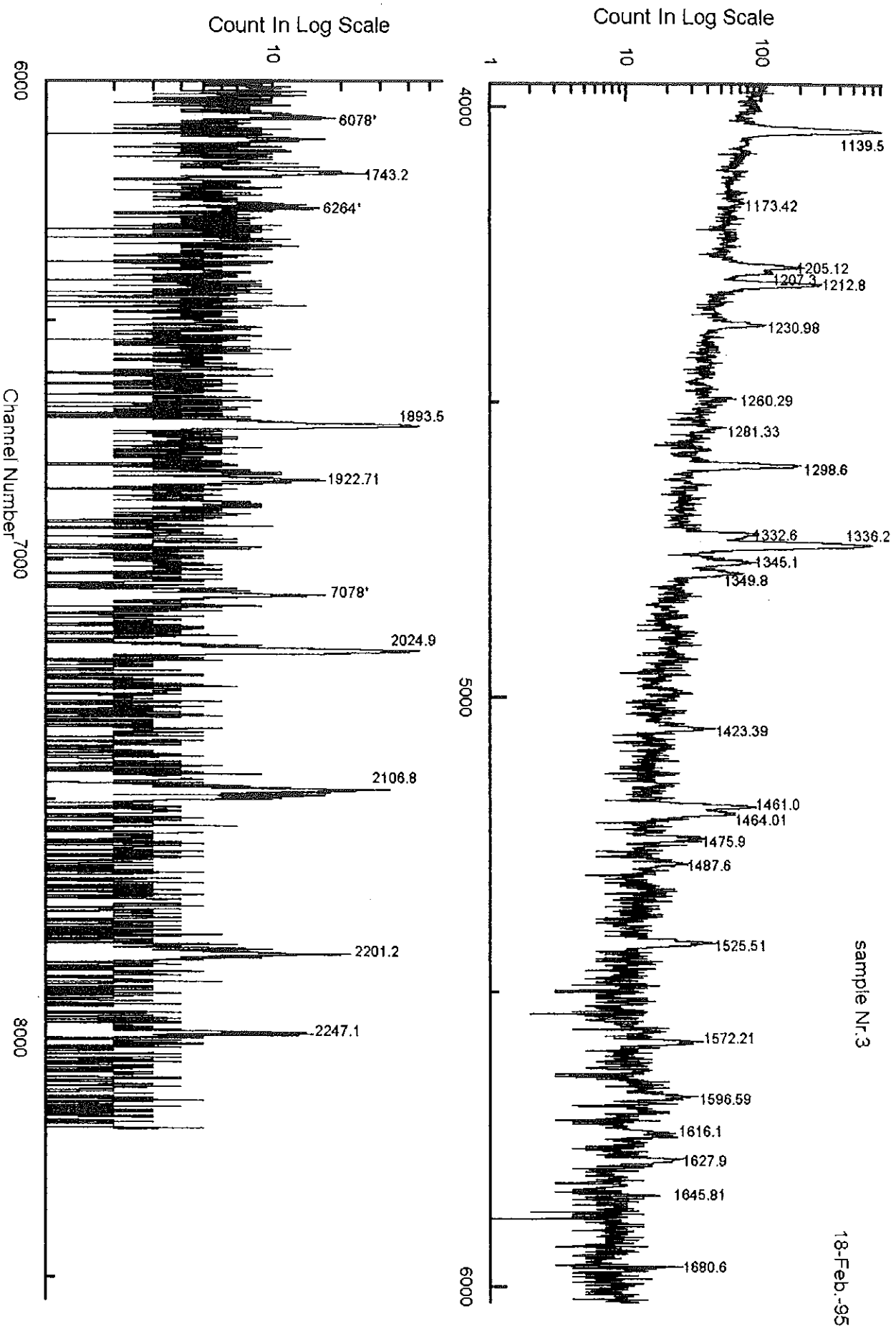

Fig.B.3 The second half of the spectrum from sample Nr.3

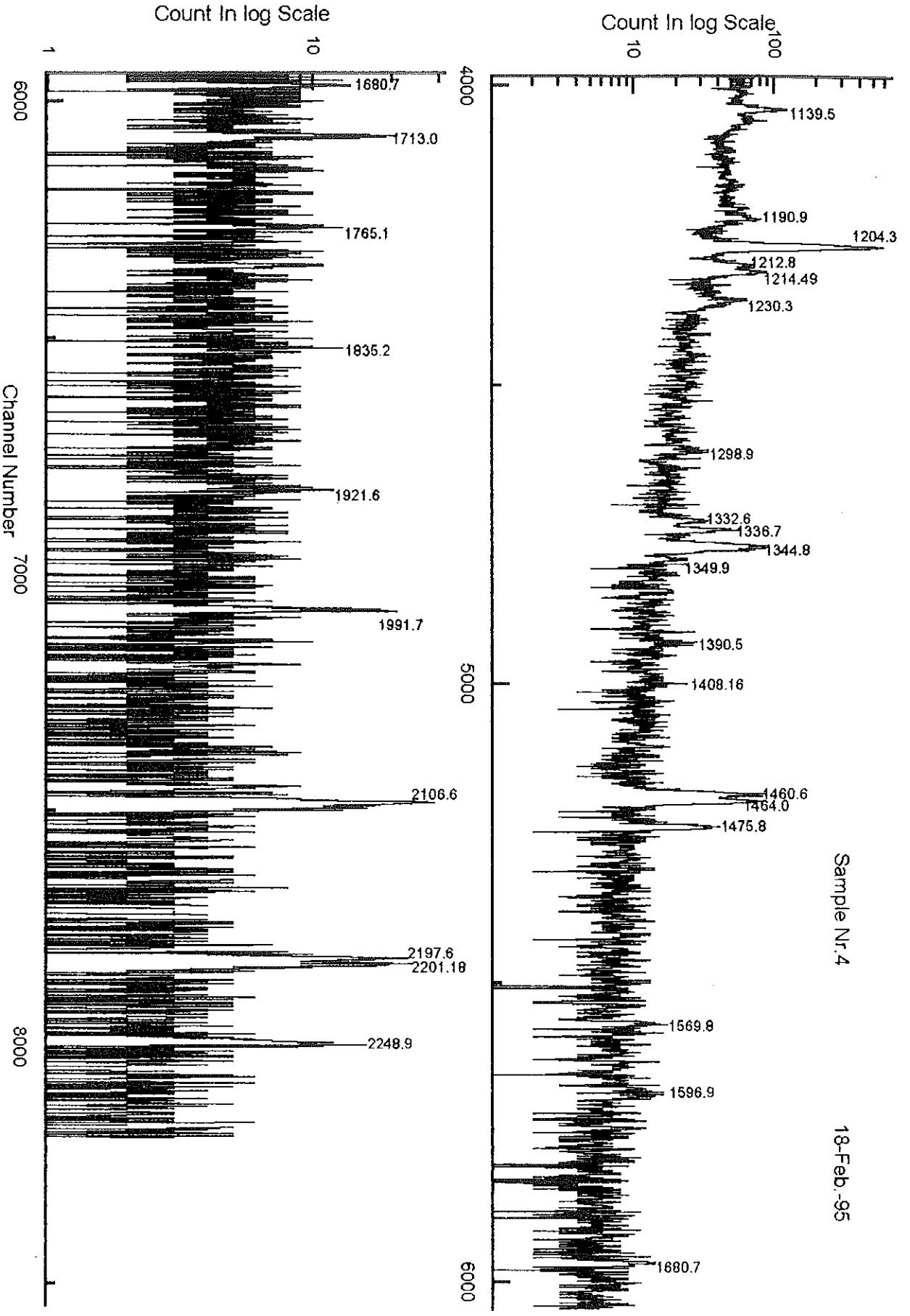

Fig.B.4 The second half of the spectrum from sample Nr.4

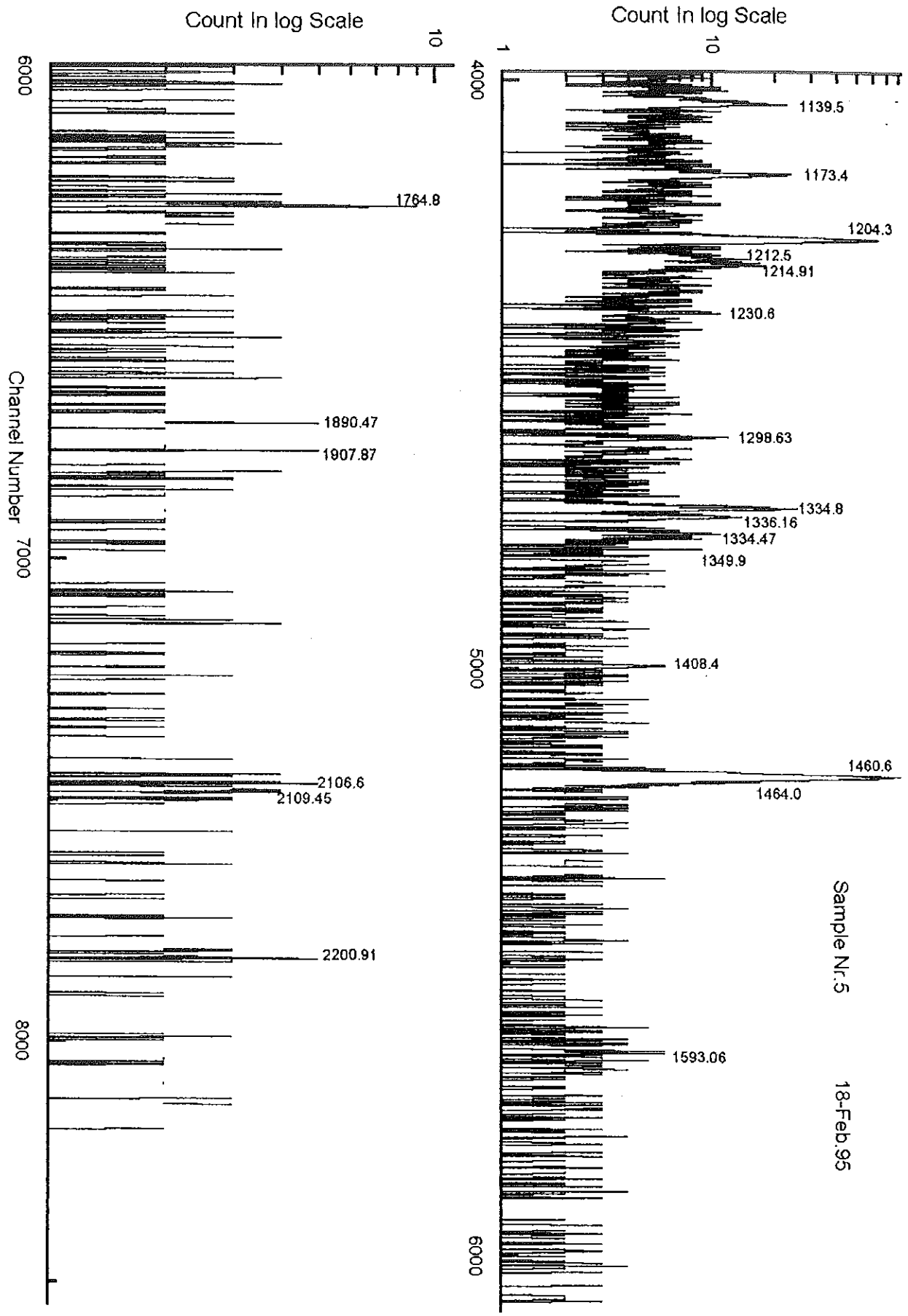

Fig.B.5 The second half of the spectrum from sample Nr.5

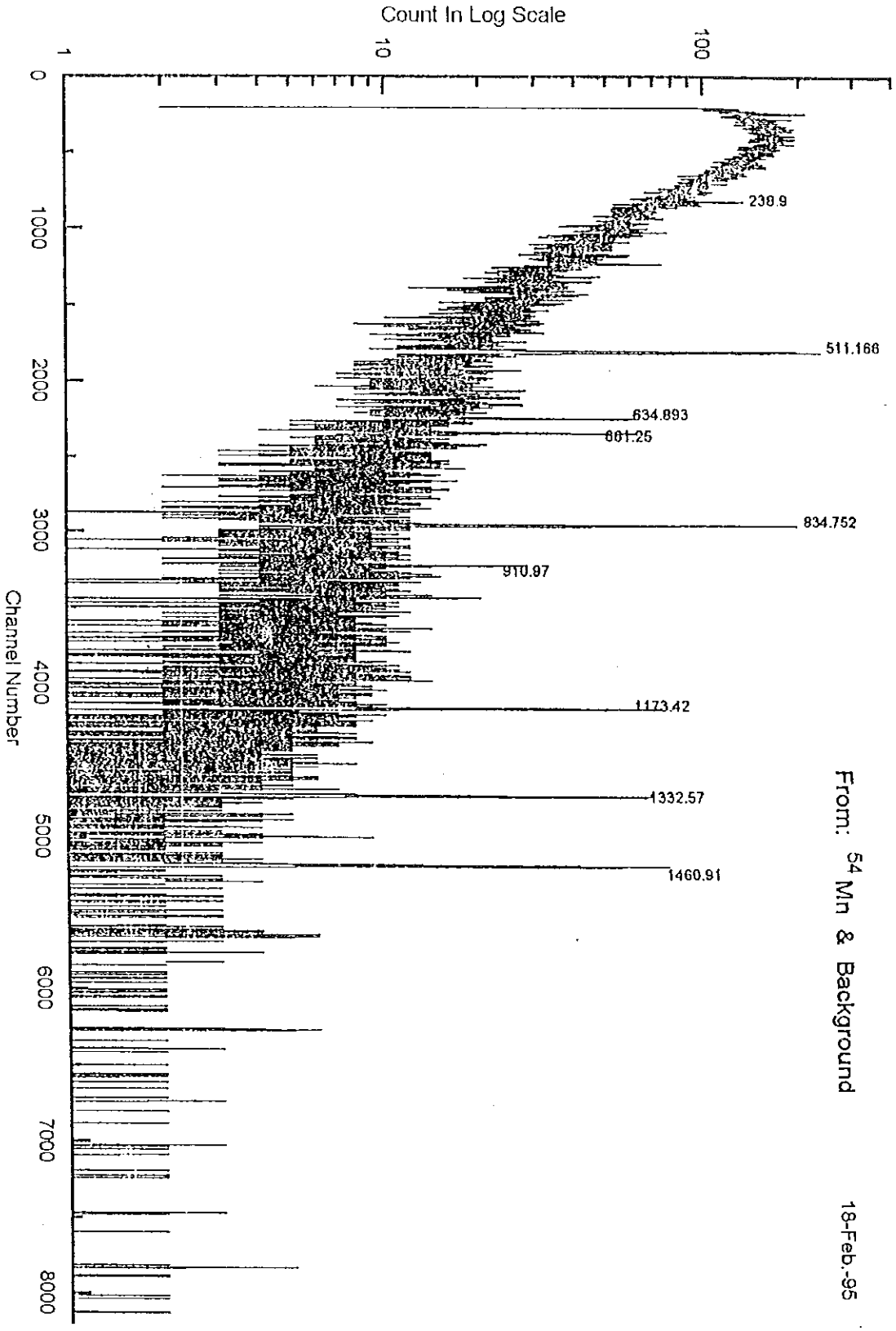

Appendix C. The background of the room and a peak from activity calibration source.